European Journal of Medicinal Chemistry 249 (2023) 115144

Contents lists available at ScienceDirect

European Journal of Medicinal Chemistry

journal homepage: www.elsevier.com/locate/ejmech

Research paper

Discovery of 4-oxo-*N*-phenyl-1,4-dihydroquinoline-3-carboxamide derivatives as novel anti-inflammatory agents for the treatment of acute lung injury and sepsis

Jun Yang [a,1], Minxiu Wang [a,1], Yulan Xu [a], Jing Liao [a], Xiang Li [a], Ying Zhou [a], Jintian Dai [b], Xiaobo Li [a], Pan Chen [a,d], Gaozhi Chen [a], Won-Jea Cho [d], Nipon Chattipakorn [e], Aleksandr V. Samorodov [f], Valentin N. Pavlov [f], Yi Wang [a,**], Guang Liang [a,b,c,***], Qidong Tang [a,b,*]

[a] Chemical Biology Research Center, School of Pharmaceutical Sciences, Wenzhou Medical University, Wenzhou 325035, Zhejiang, China
[b] Wenzhou Institute, University of Chinese Academy of Sciences, Wenzhou 325024, Zhejiang, China
[c] School of Pharmacy, Hangzhou Medical College, Hangzhou 311399, Zhejiang, China
[d] College of Pharmacy, Chonnam National University, Gwangju, 61186, South Korea
[e] Cardiac Electrophysiology Research and Training Center, Faculty of Medicine, Chiang Mai University, Chiang Mai 50200, Thailand
[f] Department of Pharmacology, Bashkir State Medical University, Ufa City 450005, Russia

ARTICLE INFO

Handling Editor: Z Liu

Keywords:
4-oxo-*N*-phenyl-1,4-dihydroquinoline-3-carboxamide derivatives
Acute lung injury
Sepsis
Anti-inflammatory
SARs

ABSTRACT

Acute lung injury (ALI) and sepsis, characterized by systemic inflammatory response syndrome, remain the major causes of death in severe patients. Inhibiting the release of proinflammatory cytokines is considered to be a promising method for the treatment of inflammation-related diseases. In this study, a total of 28 4-oxo-*N*-phenyl-1,4-dihydroquinoline-3-carboxamide derivatives were designed and synthesized and their anti-inflammatory activities in J774A.1 were evaluated. Among them, derivative **13a** was found to significantly inhibit lipopolysaccharide (LPS)-induced expression of the proinflammatory cytokines interleukin-6 (IL-6) and tumor necrosis factor-α (TNF-α) on J774A.1, THP-1 and LX-2 cells, and inhibited the activation of the NF-κB pathway. Furthermore, administration of **13a** *in vivo* significantly improved the symptoms in LPS-induced ALI mice, including alleviation of pathological changes in the lung tissue, reduction of pulmonary edema, and inhibition of macrophage infiltration. Moreover, the administration of **13a** *in vivo* significantly promoted survival in LPS-induced sepsis mice. **13a** demonstrated favorable pharmacokinetic properties with $T_{1/2}$ value of 11.8 h and F value of 36.3%. Therefore, this study has identified a novel 4-oxo-*N*-phenyl-1,4-dihydroquinoline-3-carboxamide derivative, **13a**, which is an effective anti-inflammatory agent. The findings have laid a foundation for the further development of agents to treat ALI and sepsis.

1. Introduction

Acute lung injury (ALI) and sepsis are common life-threatening diseases caused by acute inflammation [1,2]. The clinical description of ALI has been established for >50 years. ALI is characterized by acute, progressive respiratory distress and persistent hypoxemia. However, advances in its treatment can only be traced back >20 years [3]. Sepsis is an organ dysfunction syndrome caused by the dysregulation of the host response system to systemic infection. In ALI and sepsis, multiple proinflammatory cytokines are synthesized and released from the innate immune system as a defense mechanism against invading pathogens and infections. However, large amounts of proinflammatory cytokines are systemically released during immune activation, which often leads to widespread inflammation, multi-organ failure, and even death.

* Corresponding author. Chemical Biology Research Center, School of Pharmaceutical Sciences, Wenzhou Medical University, Wenzhou 325035, Zhejiang, China.
** Corresponding author. Chemical Biology Research Center, School of Pharmaceutical Sciences, Wenzhou Medical University, Wenzhou 325035, Zhejiang, China.
*** Corresponding author. Chemical Biology Research Center, School of Pharmaceutical Sciences, Wenzhou Medical University, Wenzhou 325035, Zhejiang, China.
E-mail addresses: yi_wang1122@163.com (Y. Wang), wzmcliangguang@163.com (G. Liang), tangqidongcn@126.com (Q. Tang).
[1] These authors contribute equally to this work.

https://doi.org/10.1016/j.ejmech.2023.115144
Received 9 October 2022; Received in revised form 9 January 2023; Accepted 19 January 2023
Available online 23 January 2023

Currently, ALI and sepsis are recognized as important global healthcare issues [4,5].

Lipopolysaccharide (LPS), an endotoxin derived from gram-negative bacteria, is a potent inducer of acute inflammation, which can cause ALI and sepsis (Fig. 1) [6,7]. In addition, LPS is a powerful activator of toll-like receptor 4 (TLR4). After stimulation with LPS, the receptor polymer TLR4/MD2/LPS was formed, wherein myeloid differentiation 2 (MD2) is an essential recognized helper receptor for TLR4 to recognize LPS [8,9]. The stimulation of LPS triggers the TLR4/MD2 downstream signal transduction, such as the activation of the NF-κB pathway, which then upregulates the expression of inflammation-related genes and increases the release of proinflammatory cytokines, such as cytokine interleukin-6 (IL-6) and tumor necrosis factor-alpha (TNF-α). Cumulatively, these factors lead to the occurrence of inflammatory-related diseases [10–13].

Presently, there is no approved drugs for ALI and sepsis despite several candidates having entered to the clinical study, such as L-citrulline, Aspirin, Ibuprofen and Resatorvid as shown in Fig. S1 [14–17]. Most of the reported therapeutic agents are in the stage of preclinical research and biological activity evaluation, such as Isofraxidin and Shikonin, Chalcone derivatives **7w**, fisetin derivatives **5e**, small molecule compounds 2-Methylquinazolin-4(3*H*)-one and 4-Octyl Itaconate [18–22]. Drug therapy for ALI and sepsis is also extremely limited owing to drug resistance and toxicity issues. Therefore, it is very important to develop an effective anti-inflammatory drug with a new structural scaffold [23]. Inhibiting the release of proinflammatory cytokines may thus be a potential strategy for the treatment of inflammatory-related diseases [24].

Our research group has been undertaking the works involved in designing, synthesizing and evaluating anti-inflammatory drugs for over a decade. By applying the combination principle, several derivatives with anti-inflammatory properties have been designed and synthesized, such as *N*-[3-(1*H*-indol-5-yl)-1*H*-indazol-5-yl]-2,6-dichlorobenzamide (**22m**) and 5-(3,3-dimethylureido)-*N*-[4-(4-methylpiperazin-1-yl) phenyl]-1-[4-(trifluoromethyl)benzyl]-1*H*-indole-2-carboxamide (**14g**) through the combination of indole, indazole, or benzyl group and so on, as depicted in Fig. 2 [25,26]. Analyses of the structures of **22m** and **14g** revealed that they both contained fragments of arylamide, which resembles paracetamol, a drug commonly used in clinical practice for its antipyretic and analgesic properties [27]. Similar to arylamide, paracetamol is composed of a fragment of 4-(hydroxyphenyl)amide. Accordingly, we designed the molecular skeleton containing three portions of moiety A (A1 and A2), B, and C as shown in Fig. 3. By transferring the oxygen atom in the 4th position (moiety A1) to the 3rd position (moiety A2) of phenyl amide, two types of molecular skeletons were designed. We found that quinolone antibacterial drugs (Difoxacine, Levofloxacin, Ozenoxacin, etc.) basically have quinolone structure. Difloxacin was mainly used for animal bacterial infection in a clinical setting [28]. Levofloxacin and Ozenoxacin have been reported to have anti-inflammatory effects, and so we introduced quinolone structure to the molecular skeletons to serve as moiety B [29,30]. Different substituents were introduced into the phenyl group of moiety B to study their effects on activity. In addition, we found that some compounds had the 6,7-dimethoxyquinazoline structure, such as the epidermal growth factor receptor (EGFR) inhibitor Gefitinib. EGFR signaling has been implicated in inflammatory disease [31,32]. At the same time, we also found that some reported anti-inflammatory compounds containing the quinazoline structure, such as **6b** in Fig. 2 [33]. And so, we introduced 6,7-dimethoxyquinazoline or 6,7-dimethoxyquinoline to moiety C with the assistance of the bioisosterism principle. Therefore, two types of target compounds were designed according to the combination principle.

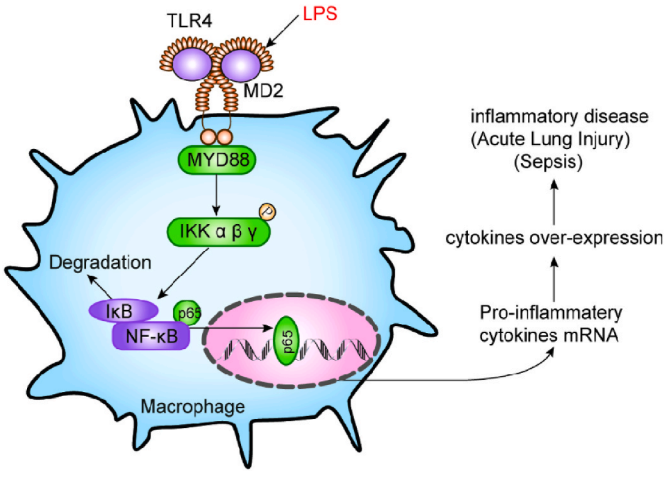

Fig. 1. NF-κB pathway, an important pathway in LPS-induced TLR4/MD2 signaling in ALI and sepsis.

In this study, we designed and synthesized a total 28 4-oxo-*N*-phenyl-1,4-dihydroquinoline-3-carboxamide derivatives and then evaluated the inhibitory effect of these derivatives on the release of proinflammatory cytokines *in vitro*. Among these, **13a** exhibited the best inhibitory effect *in vitro*, and could inhibit the activation of the NF-κB pathway. Moreover, **13a** could improve the symptoms of LPS-induced ALI and sepsis *in vivo*.

2. Results

2.1. Chemistry

The synthetic route for 4-oxo-*N*-phenyl-1,4-dihydroquinoline-3-carboxamide derivatives is illustrated in Scheme 1. Briefly, 1-(2-chlorophenyl)ethan-1-one (**1**) was reacted with dimethyl carbonate and sodium hydride (NaH) in chlorobenzene to obtain methyl 3-(2-chlorophenyl)-3-oxopropanoate (**2**). Intermediate **2** was reacted with *N,N*-dimethylformamide dimethyl acetal (DMF-DMA) in toluene to get methyl (*Z*)-2-(2-chlorobenzoyl)-3-(dimethylamino)acrylate (**3**). Derivatives **4a**–**4g** were obtained via nucleophilic substitution reactions of intermediate **3** in toluene with aminobenzene of different substituents, which were, in turn, converted to intermediates **5a**–**5g** by reacting with cesium carbonate (Cs_2CO_3) and potassium carbonate (K_2CO_3). Subsequently, **5a**–**5g** were hydrolyzed under alkaline conditions to derive **6a**–**6g**. 4-Chloro-6,7-dimethoxyquinoline (**7a**) or 4-chloro-6,7-dimethoxyquinazoline (**7b**) was reacted with 3-nitrophenol (**8a**) or 4-nitrophenol (**8b**) using nucleophilic substitution reactions to acquire the intermediates **9a**–**9d**. Later, **10a**–**10d** were prepared via the reduction of the nitro groups of **9a**–**9d** using catalytic iron and ammonia chloride in ethanol. Finally, the corresponding amines (**10a**–**10d**) were reacted with the corresponding acids (**6a**–**6g**) to produce **11a**–**11g, 12a**–**12g, 13a**–**13g**, and **14a**–**14g** using 2-(7-azab-enzotriazol-1-yl)-*N,N,N′,N′*-tetramethyluronium hexafluorophosphate (HATU) as the condensation agent under the presence of *N*-ethyl-*N,N*-diisopropylamine (DIPEA) in *N,N*-dimethylformamide (DMF).

Reagents and conditions: (i) NaH, tetrahydrofuran (THF), 85 °C, 2.5 h. (ii) DMF-DMA, toluene, 120 °C, 2 h (iii) Different substituted aminobenzenes, toluene, 110 °C, 5.5 h. (iv) Cs_2CO_3, K_2CO_3, toluene, 150 °C, 10 h. (v) NaOH, 1,4-dioxane, 85 °C, 2 h. (vi) Na_2CO_3, NaI, chlorobenzene, 130 °C, 12 h (vii) Catalytic iron, ethanol, 50 °C, 6 h (viii) DMF, HATU, DIPEA, room temperature, 16 h.

2.2. Biological evaluation

2.2.1. Preliminary evaluation of the derivatives inhibiting LPS-induced release of TNF-α and IL-6

LPS plays a key role in the progression of the systemic inflammatory response, especially the release of proinflammatory cytokines such as IL-6 and TNF-α [34–36]. Therefore, the effects of 4-oxo-*N*-phenyl-1,

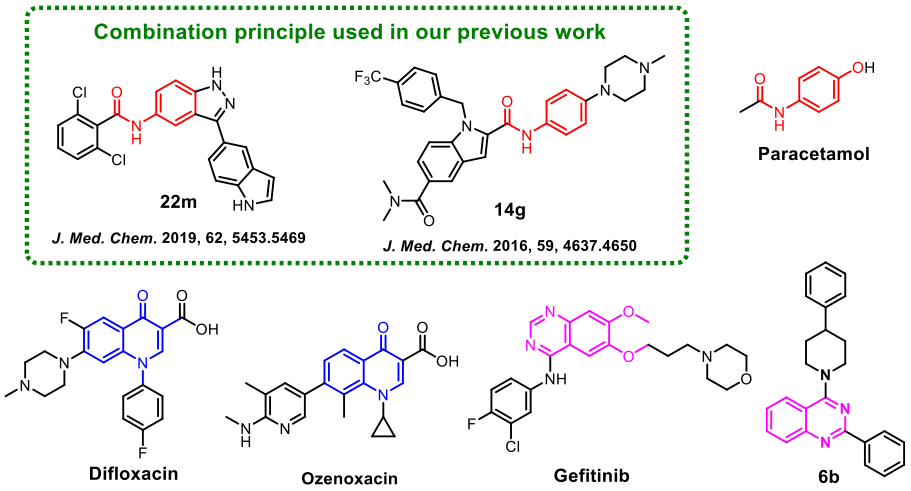

Fig. 2. Typical structures. **22m** and **14g** are the anti-inflammatory agents reported by our group based on the combination principle. Representative agents (paracetamol, difloxacin, ozenoxacin, gefitinib, and **6b**) drew our attention to this study.

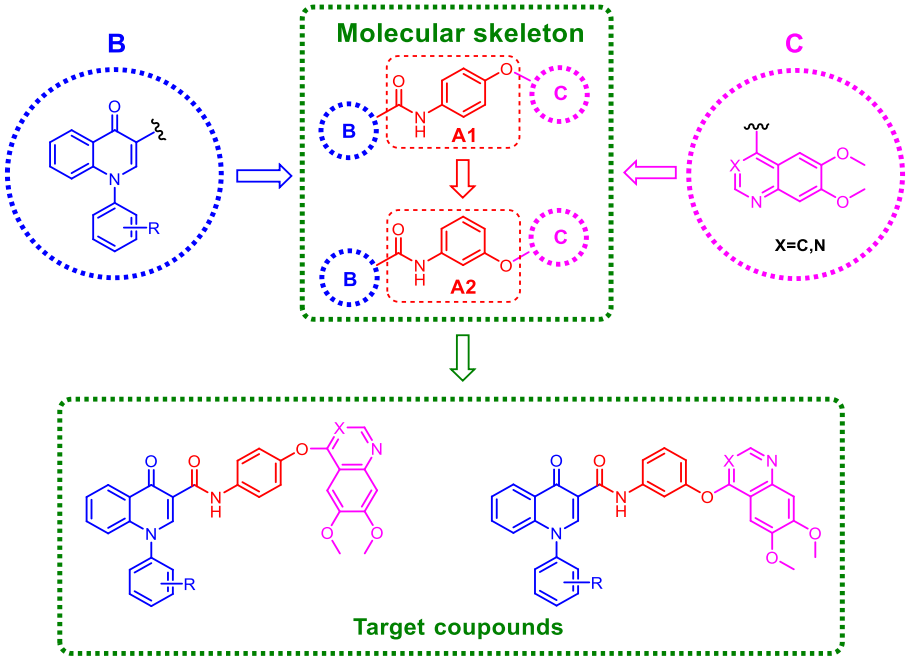

Fig. 3. Design and modification strategy based on the combination principle.

4-dihydroquinoline-3-carboxamide derivatives on LPS-induced release of proinflammatory cytokines IL-6 and TNF-α by J774A.1 were evaluated [37,38]. The inhibitory effects of all synthesized compounds were screened using an enzyme-linked immunosorbent assay (ELISA), and the inhibitory abilities are presented in Table 1. First, J774A.1 macrophages were preincubated with the derivatives at a concentration of 10 μM for 30 min. The macrophages were then challenged with LPS (0.5 μg/mL) for 24 h at 37 °C under 5% CO_2. The results showed that most of the derivatives inhibited the LPS-induced release of TNF-α and IL-6. With regard to IL-6, compounds **11g**, **13a, 13b,** and **13f** showed strong inhibitory effects, whereas compounds **13a**, **13b**, **13f,** and **13g** significantly inhibited the release of TNF-α. Among these compounds, **13a** and **13b** exhibited the strongest inhibitory effect on LPS-induced TNF-α (82.58% and 83.07%, respectively) and IL-6 (75.05% and 77.39%, respectively) expression.

2.2.2. *Structure-activity relationships*

In this study, some obvious structure-activity relationships (SARs) were discerned. As shown in Table 1, when moiety A was A2, the compounds exhibited a weaker inhibitory effect on TNF-α; for example, only four compounds in **11a**–**12g** showed anti-inflammatory effects. However, the compounds comprising moiety A1 demonstrated a significantly enhanced inhibitory effect on the release of TNF-α; for example, 11 compounds in **13a**–**14g** displayed strong anti-inflammatory activities. Unlike the above scenario, the compounds consisting of moiety A1 as well as those consisting of moiety A2 showed an inhibitory effect on the release of IL-6. However, after careful comparison, compounds comprising moiety A1 were found to exert a stronger anti-inflammatory effect on IL-6. For example, the inhibitory effects of **13a** (75.05%) and **14b** (56.98%) were significantly stronger than those of **11a** (44.84%) and **12b** (45.44%).

The test results indicated that the changes in the substituent introduced in moiety B were closely related to the alterations in the activities

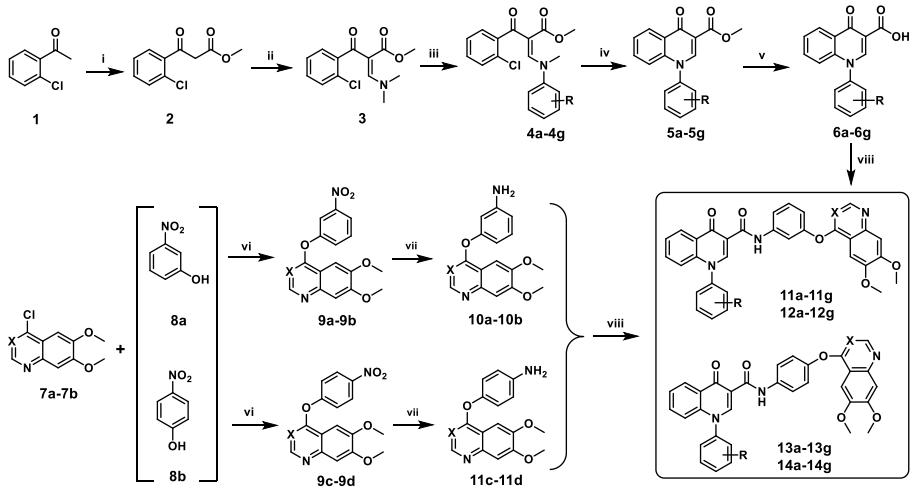

Scheme 1. Stepwise synthetic route for the target compounds.

Table 1
Structure and anti-inflammatory screening of compounds.

Compound	R	X	(%) inhibition (10 μM)[a]	
			IL-6	TNF-α
11a	4-H	C	44.84 ± 7.92	NA[b]
11b	4-F	C	51.29 ± 5.20	NA
11c	4-Cl	C	60.17 ± 0.50	NA
11d	4-Br	C	37.09 ± 2.75	NA
11e	2-F-4-Br	C	52.89 ± 3.17	NA
11f	3-Cl-4-F	C	49.71 ± 2.54	32.64 ± 4.12
11g	4-OCF_3	C	66.37 ± 4.05	33.29 ± 12.01
12a	4-H	N	42.44 ± 1.94	NA
12b	4-F	N	45.44 ± 5.07	NA
12c	4-Cl	N	32.33 ± 4.69	NA
12d	4-Br	N	20.42 ± 2.25	NA
12e	2-F-4-Br	N	NA	NA
12f	3-Cl-4-F	N	33.88 ± 11.92	35.97 ± 11.16
12g	4-OCF_3	N	10.39 ± 2.86	7.66 ± 8.42
13a	4-H	C	75.05 ± 1.63	82.58 ± 1.17
13b	4-F	C	77.39 ± 3.55	83.07 ± 1.15
13c	4-Cl	C	32.04 ± 8.48	63.48 ± 1.30
13d	4-Br	C	41.72 ± 4.38	71.67 ± 4.49
13e	2-F-4-Br	C	26.71 ± 1.04	NA
13f	3-Cl-4-F	C	62.24 ± 6.45	67.65 ± 3.929
13g	4-OCF_3	C	50.49 ± 3.85	67.61 ± 4.692
14a	4-H	N	38.10 ± 10.57	30.53 ± 12.49
14b	4-F	N	56.98 ± 11.54	47.99 ± 8.930
14c	4-Cl	N	30.46 ± 8.956	NA
14d	4-Br	N	NA	22.35 ± 6.431
14e	2-F-4-Br	N	13.28 ± 4.81	NA
14f	3-Cl-4-F	N	39.56 ± 6.73	48.03 ± 5.166
14g	4-OCF_3	N	35.93 ± 2.94	54.90 ± 4.757

[a] Statistical significance relative to LPS group was indicated.
[b] NA indicates no activity.

of these derivatives. Generally, when the atomic radius of the para-substituent of the phenyl group in moiety B was large, the inhibitory effects of the compounds on the release of proinflammatory cytokines were poor. For example, when the substituent in moiety B was 4-Br (**11d, 12d, and 14d**), the effects of inhibition were poor both in IL-6 and TNF-α; the inhibition rate of IL-6 was 37.09%–41.72% and that of TNF-α was NA–22.35%. However, when a substituent with a small atomic radius, such as 4-H (**11a** and **13a**) or 4-F (**11b** and **13b**), was introduced into moiety B, the activities were improved and the inhibition rate of IL-6 was 44.84%–77.39%. The inhibitory effects on TNF-α also showed a similar pattern, with **11f**, **12f**, **13b,** and **14b**, demonstrating stronger inhibitory effects than other compounds in the same series. Moreover, when two substituents were introduced, the inhibitory effects of the compounds on IL-6 were decreased.

Finally, when X in moiety C was a carbon atom, the activities of the compounds inhibiting the release of proinflammatory cytokines were significantly stronger than when X was a nitrogen atom. For example, the inhibitory effects of **11f** (49.71%, 32.64%), **13c** (32.04%, 63.48%), and **13d** (41.72%, 71.67%) for IL-6 and TNF-α were stronger than those of **12f** (33.88%, 35.97%), **14c** (30.46%, NA), and **14d** (NA, 22.35%).

In conclusion, among the compounds screened, **13a** and **13b** were found to display the most significant inhibitory effects on IL-6 and TNF-α. Analyzing the structures of these two compounds revealed that both had moiety A1 and that X in moiety C comprised carbon atoms. The only difference was that in moiety B, R of **13a** was 4-H and R of **13b** was 4-F. Interestingly, the atomic radius of the F atom was very close to that of the H atom, and they were very small. The 4-oxo-*N*-phenyl-1,4-dihydroquinoline-3-carboxamide derivatives **13a** and **13b** appear to be promising compounds.

Subsequently, cytotoxicity experiments were performed on compounds with strong anti-inflammatory activities. As expected, **13a** and **13b** did not exhibit cytotoxicity at 10 μM concentration in J774A.1 macrophage (Fig. 4). Therefore, **13a** and **13b** were selected to investigate the potential dose-dependent inhibition of cytokines.

2.2.3. Dose-dependent inhibition of IL-6 and TNF-α release by active compounds

The denoting 50% inhibition (IC_{50}) concentrations of two active compounds (**13a** and **13b**) were obtained using dose-response experiments. As shown in Fig. 5A and B, **13a** and **13b** inhibited LPS-induced release of proinflammatory cytokines in a dose-dependent manner. Both for IL-6 and TNF-α, the IC_{50} values of **13a** (1.332, 2.403 μM) were lower than those of **13b** (2.333, 3.460 μM). Nextly, we evaluated the effect of **13a** on LPS-induced release of pro-inflammatory cytokines IL-6 and TNF-α from THP-1 (Fig. 5C and E) and LX-2 (Fig. 5D and F). This

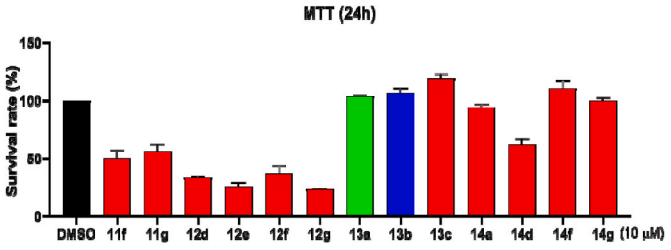

Fig. 4. Cell viability was detected by MTT assay and expressed as the percentage of the control group (DMSO).

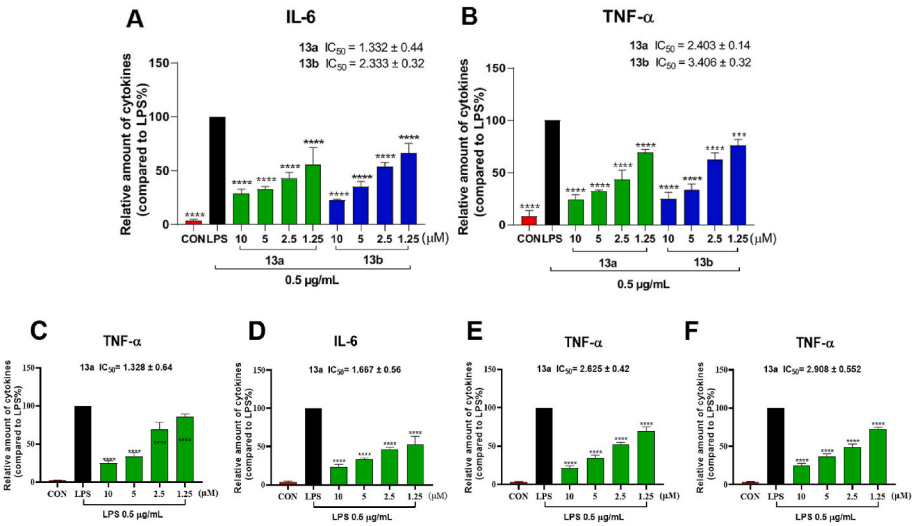

Fig. 5. 13a and **13b** inhibited the LPS-induced release of proinflammatory cytokines in a dose-dependent manner. First, J774A.1 macrophages were preincubated with **13a** and **13b** in decreasing concentrations (10, 5, 2.5, 1.25 μM) for 30 min and then stimulated with LPS (0.5 μg/mL) for 24 h. THP-1 and LX-2 were preincubated with **13a** in decreasing concentrations (10, 5, 2.5, 1.25 μM) for 30 min and then stimulated with LPS (0.5 μg/mL) for 24 h. The contents of IL-6 (A, C, E) and TNF-α (B, D, F) were detected by ELISA. Data were expressed as the mean ± SEM of 3 independent experiments. When compared with the LPS group, the difference was found to be statistically significant (***$p < 0.001$ and ****$p < 0.0001$).

finding signified that **13a** had a better inhibitory effect at lower concentrations and has an anti-inflammatory effect on human cells, hence, 4-oxo-*N*-phenyl-1,4-dihydroquinoline-3-carboxamide derivative **13a** was selected for subsequent experiments.

2.2.4. *Dose-dependent inhibition of some proinflammatory cytokines at transcript levels by **13a***

LPS induces inflammation via the TLR4/MD2 cascade. To investigate the anti-inflammatory mechanism of **13a** in J774A.1 and THP-1, the effect of the compound on the gene expression of TLR4/MD2-dependent inflammatory cytokines was observed [39–41]. The alterations in some proinflammatory cytokines at the gene transcription level were measured using real-time quantitative PCR (RT-qPCR). The findings implied that **13a** inhibited the transcription of IL-6, TNF-α, and IL-1β in LPS-induced J774A.1 and THP-1 in a dose-dependent manner (Fig. 6A, B, 6C, 6D, 6E and 6F). The above data suggest that **13a** exerts its anti-inflammatory effect by inhibiting the transcription of proinflammatory genes.

2.2.5. *Primary test on stability of **13a** in vitro*

To investigate the stability of the **13a** *in vitro*, a primary test carried out by using UV–visible absorption spectra similar to the method we recently reported [42]. **13a** was dissolved in phosphate buffer (pH 7.4). And then, the optical density (OD) values were measured by using ultraviolet–visible (UV–visible) within 30 min as shown in Fig. 7. Our data revealed that the OD value of **13a** did not change with time, which indicated its stability in this method.

2.2.6. *Inhibition of LPS-induced activation of NF-κB pathway in J774A.1 macrophage by **13a***

LPS-induced release of proinflammatory cytokines can be regulated by the activation of the NF-κB pathway. Phosphorylation of p65 and degradation of IκB-α are necessary steps for the activation of this pathway [43,44]. Therefore, the effect of **13a** on the activation of the

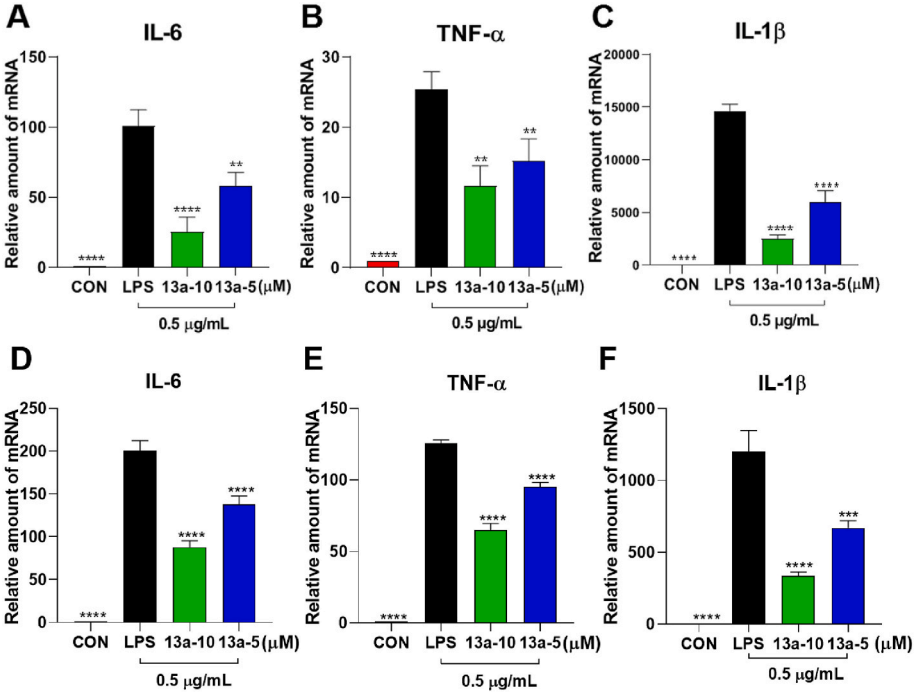

Fig. 6. Derivative **13a** inhibited LPS-induced transcription of proinflammatory genes in J774A.1 and THP-1. J774A.1 and THP-1 were pretreated with **13a** in decreasing concentrations (10 and 5 μM) for 0.5 h, followed by stimulation with LPS (0.5 μg/mL) for 6 h. (A, D) IL-6, (B, E) TNF-α, and (C, F) IL-1β were measured by RT-qPCR. Data were expressed as the mean ± SEM of 3 independent experiments and normalized to the β-actin and control group (**$p < 0.01$, ***$p < 0.001$, and ****$p < 0.0001$ when compared to LPS).

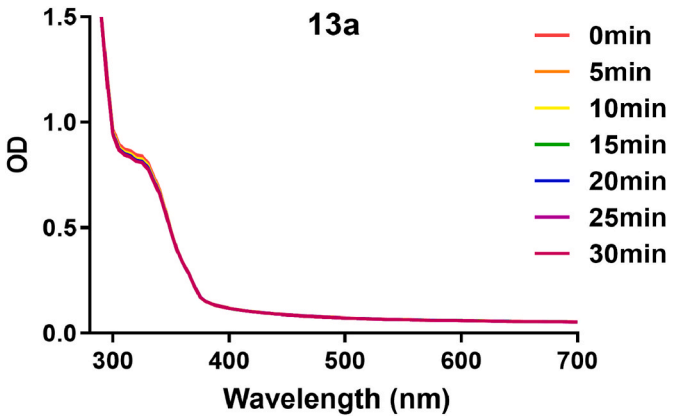

Fig. 7. The UV–visible absorption spectra of the compounds **13a** in the stability test.

NF-κB pathway was assessed. In J774A.1 macrophages treated with **13a**, both LPS-induced phosphorylation of p65 (p-p65) and degradation of IκB-α was found to be inhibited in a dose-dependent manner (Fig. 8A, C, and 8D). Phospho–NF–κB P65 (Ser536) (93H1) Rabbit mab #3303 was used to measure phosphorylation on p65. Ser536 is an important phosphorylation site of RelA/p65, which can be phosphorylated by a variety of phosphorylation kinases, such as IκB kinase (IKK), TANK binding kinase (TBK1), ribosomal subunit kinase I (RSKI), etc. Consistent with the above results, **13a** significantly reduced the LPS-induced nuclear translocation of p65 in J774A.1 macrophages (Fig. 8B and E). These findings imply that **13a** may exert its anti-inflammatory effects by inhibiting the activation of the NF-κB pathway.

*2.2.7. The protective effect of **13a** on LPS-induced ALI in mice*

The manifestations of LPS-induced ALI were hypercellularity, alveolar wall thickening, pulmonary edema, destruction of normal lung architecture, etc. [45–47]. The therapeutic effect of **13a** in LPS-induced ALI mice was assessed. One experimental concentration (20 mg/kg) was used to verify the effect of **13a**. Dexamethasone (DXMS, 20 mg/kg), whose main pharmacological effects are anti-inflammatory, antitoxic, antiallergic, and anti-rheumatic, was used for positive comparison. Histological analysis disclosed that the LPS-induced mice exhibited significant structural disruption of the lung tissue and alveolar wall thickening and that these phenomena were significantly improved in **13a-** and DXMS-treated mice (Fig. 9A). The value of the lung wet/dry ratio was used to express the degree of inflammation and lung edema, and the lung wet/dry ratios of **13a**- and DXMS-treated mice were significantly lower than those of the LPS-induced mice (Fig. 9B). Furthermore, pulmonary edema was significantly improved. The total number of cells in the bronchoalveolar lavage fluid (BALF) increased significantly in the LPS-induced mice because of the acute inflammatory response, especially the number of neutrophils. Protein concentrations and number of total cells, especially the number of neutrophils, were reduced in the BALF of **13a**- and DXMS-treated mice compared with those of the LPS-induced mice, which further suggests that **13a** exerted an anti-inflammatory effect (Fig. 9C, D, and 9E). It was exciting to note that the protective effect of **13a** was close to that of DXMS in some aspects, such as wet/dry ratio (B) and neutropenia (E), and even better than that of DXMS in some aspects, such as protein concentration (C) and total cell reduction (D).

Patients with ALI have been reported to demonstrate significantly elevated levels of proinflammatory cytokines in the blood circulation and in the BALF as well as increased macrophage infiltration in the lung tissue [48–50]. As expected, the levels of IL-6 and TNF-α were significantly increased in the BALF and serum of LPS-induced mice, whereas they were significantly decreased in **13a**- and DXMS-treated mice (Fig. 10A, B, 10C, and 10D). It has been reported that LPS-induced ALI mice demonstrate alterations in gene expression, which are predominantly manifested as increased expression of inflammation-related genes, such as those encoding IL-6, TNF-α, and IL-1β in the TLR4/MD2 pathway. The expression levels of IL-6 and TNF-α in the lung tissue were measured. As anticipated, LPS significantly induced the transcriptional expression of these cytokines, whereas **13a** or DXMS treatment decreased their expression (Fig. 10E and F).

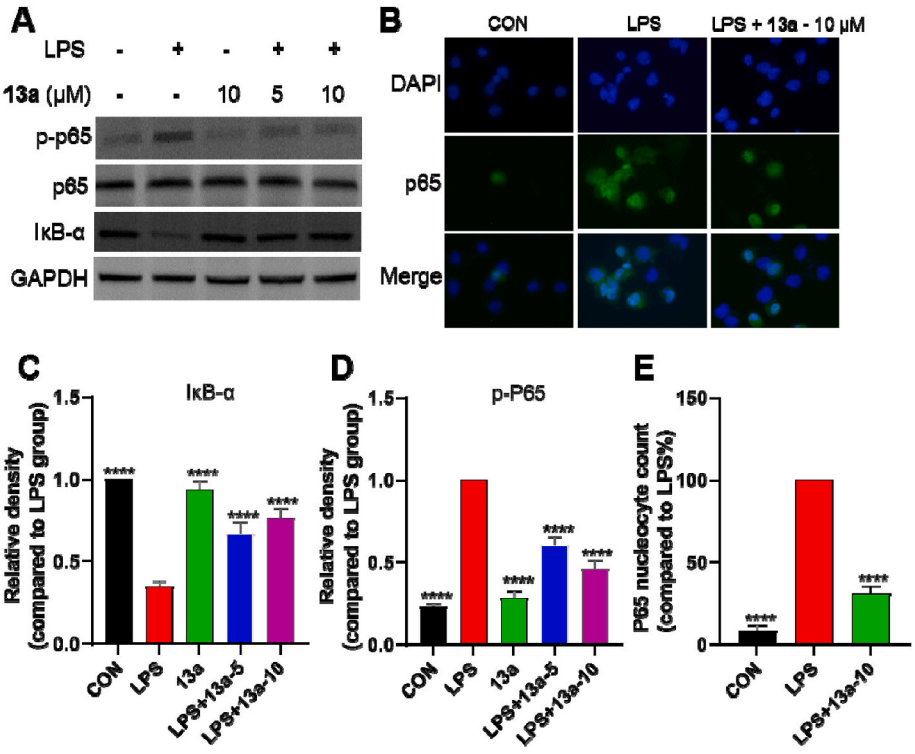

Fig. 8. Derivative **13a** may exert an anti-inflammatory effect by inhibiting the activation of the LPS-induced NF-κB pathway. (A) J774A.1 macrophages were pretreated with **13a** for 2 h, followed by treatment with LPS (0.5 μg/mL) for 30 min. The activation of NF-κB was determined by measuring the levels of IκB-α and p-p65. GAPDH and p65 were used as the loading controls. The detection of protein levels of p-p65, p65, IκB, and GAPDH were determined by Western blotting. (B) P65 staining. Cy3-conjugated secondary antibody (Green) was positive. The cells were counterstained with DAPI (blue). (C, D) Densitometric quantification of IκB-α and p-P65. (E) Quantification of p65 nucleocyte count (****p < 0.0001 when compared to LPS).

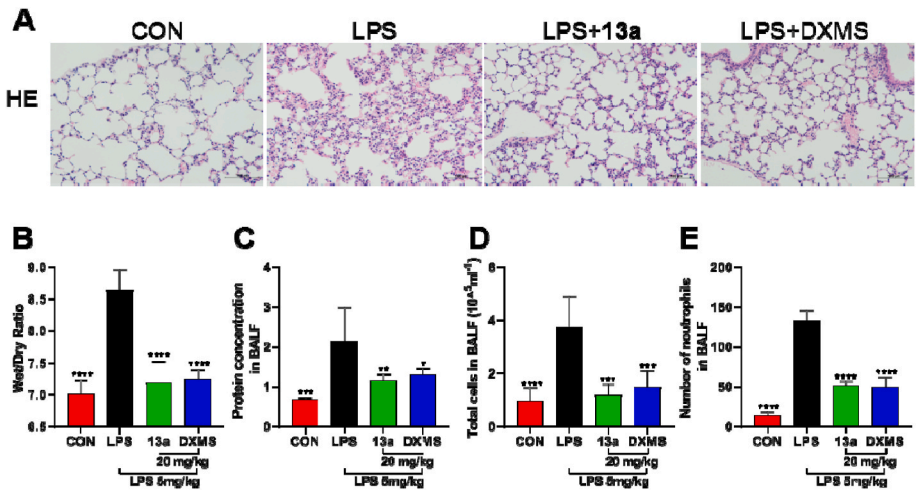

Fig. 9. Derivative **13a** protected against LPS-induced ALI in a mouse model. C57/BL6 mice were administered **13a** or DXMS (20 mg/kg) via gavage, and after 30 min, the mice were challenged with 5 mg/kg LPS via an intratracheal injection. (A) Representative histological images of mouse lung tissues. (B) Lung wet/dry ratio. (C) Protein concentration in BALF. (D) The number of total cells in BALF. (E) The number of neutrophils in BALF. Data are presented as mean ± SEM. n = 5 mice per group. (*p < 0.05, **p < 0.01, ***p < 0.001, and ****p < 0.0001 when compared with the LPS group).

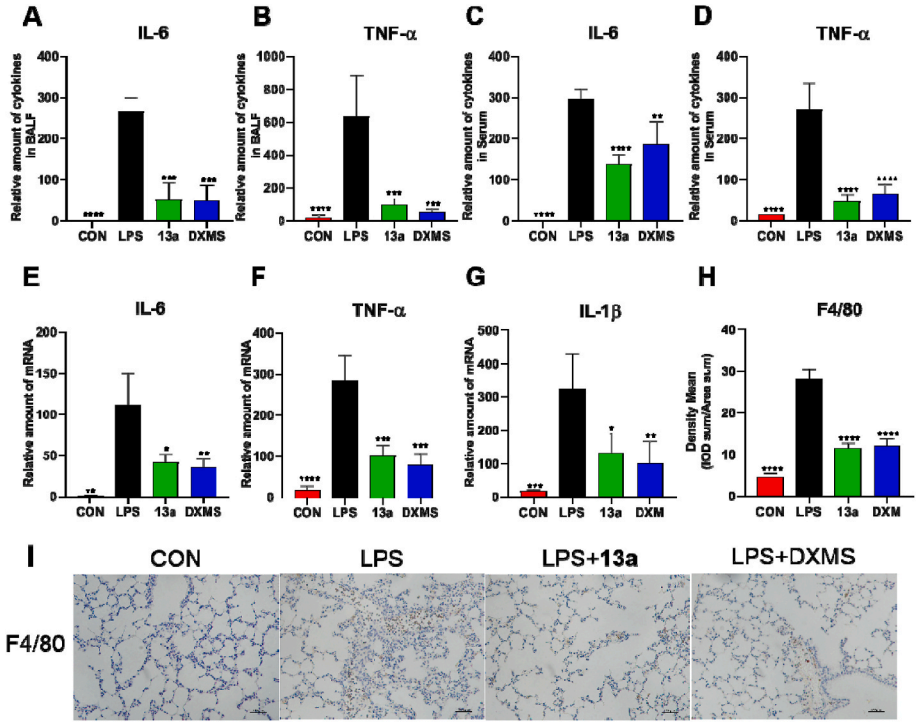

Fig. 10. Derivative **13a** treatment inhibited the production of proinflammatory cytokines and macrophage infiltration in the lungs of ALI mice. (A–D) The contents of proinflammatory cytokines in BALF were expressed as IL-6 (A) and TNF-α (B). The contents of proinflammatory cytokines in the serum were expressed as IL-6 (C) and TNF-α (D). (E–G) The transcription levels of IL-6 (E), TNF-α (F) and IL-1β (G) in the lung tissues of the mice were detected by RT-qPCR. Data were normalized to those of β-actin. (H) Quantification of F4/80 positivity. (I) Immunohistochemical staining of macrophage markers F4/80 in LPS-induced mice lung tissues. Immunoreactivity is depicted in brown (Scale bar = 100 μm). Data are presented as mean ± SEM. n = 5 mice per group. (*p < 0.05, **p < 0.01, ***p < 0.001, and ****p < 0.0001 when compared with the LPS group).

Next, macrophage-specific F4/80 antibodies were used for immunohistochemical staining to examine whether **13a** reduced macrophage infiltration. The data indicated that macrophage infiltration was significantly reduced in the lungs of **13a-** or DXMS-treated mice compared with the LPS-treated mice (Fig. 10H and K). Collectively, these data appear to confirm the protective effect of **13a** in the LPS-induced ALI model, and the effect was very close to that of DXMS and even surpassed it in some aspects. For example, as shown in Fig. 10C and D, the anti-inflammatory effect of **13a** in the blood circulation was better than that of DXMS, and it was very close to that of DXMS in other aspects, as shown in Fig. 10A, B, 10E, and 10F.

*2.2.8. Protection offered by **13a** against LPS-induced sepsis in the mouse model*

Finally, the protective effect of **13a** against LPS-induced sepsis was determined [51,52]. Observing the survival rate of LPS-induced sepsis mice revealed that the survival rate was improved in **13a**-treated mice compared with only LPS-induced mice (Fig. 11A). Furthermore, **13a** significantly improved the weight loss caused by sepsis (Fig. 11B). After 24 h of **13a** treatment, the weight of the mice began to recover and returned to normal after 6 days. However, the weight of the mice induced by LPS continued to decrease and did not start to recover until 96 h later. Moreover, there was a huge gap compared with the normal weight. The spleen, the largest lymphoid organ, is a major source of circulating proinflammatory cytokines and plays a crucial role in immunity. All experimental mice were dissected and the major organs were weighed, which revealed that the spleen was significantly enlarged in the LPS-stimulated mice under the condition of weight loss (Fig. 11C). Compared with the control group, H&E staining of the spleen tissue of the LPS group showed obvious white pulp and lymph node hyperplasia. Specifically, the periarterial lymphatic sheath was markedly thickened, and the demarcation between white and red pulp was indistinct. These phenomena were improved in the **13a**-treated group (Fig. 11D). These findings imply that **13a** also demonstrated a good therapeutic effect on

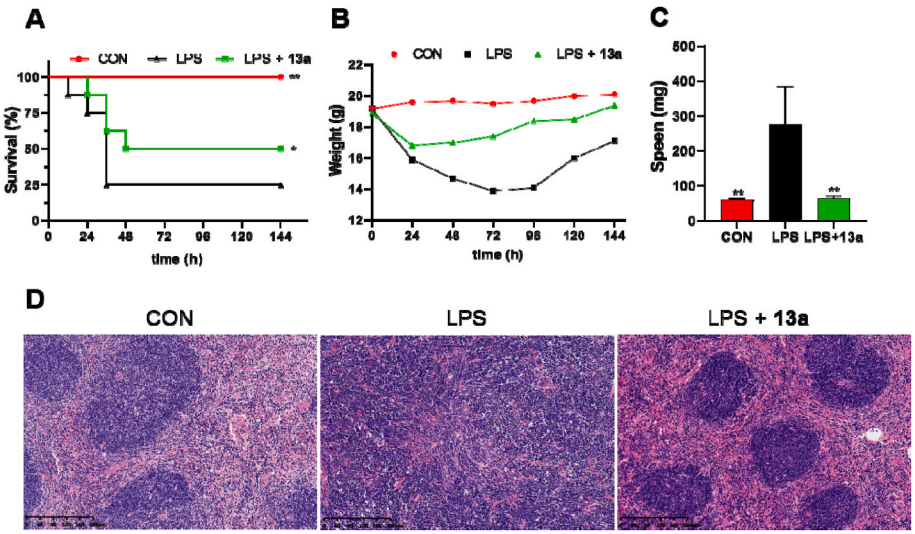

Fig. 11. Derivative **13a** protected against LPS-induced sepsis in the mouse model. C57BL/6 mice were orally administered **13a** (20 mg/kg) and then intraperitoneally injected with LPS (20 mg/kg) 1 h later. (A) Mouse survival was monitored every 12 h for 6 days. Logical survival curves were used to analyze the data (n = 12 per group). (B) The weight of the mice was monitored every 24 h for 6 days. (C–F) Weighing of the organs, such as kidney (C), liver (D), heart (E), and spleen (F) of mice. (G) Representative histological images of mouse spleen tissue (*p < 0.05, **p < 0.01, compared with the LPS group).

sepsis and may be a promising compound.

2.2.9. PK study of *13a* in rats

The pharmacokinetic properties of compound **13a** were evaluated following intravenous and oral delivery in rats, respectively. Compounds **13a** demonstrated favorable pharmacokinetic properties, with AUC value of 22,922 μg/L·h, $T_{1/2}$ value of 11.8 h following a 10 mg/kg oral dose, and F value of 36.3%, respectively (Table 2). This suggests that compound **13a** should be suitable for oral administration.

3. Conclusions

In this study, a series of 4-oxo-*N*-phenyl-1,4-dihydroquinoline-3-carboxamide derivatives were designed and synthesized and their anti-inflammatory activities were evaluated. Most compounds could effectively inhibit the release of the proinflammatory cytokines TNF-α and IL-6 caused by LPS. The structure-activity relationship study revealed that the activities of the compounds were increased in the case of a substituent with a smaller atomic radius at the 4-position of the benzene ring of moiety B. For example, when R was 4-H or 4-F, the anti-inflammatory effects were stronger than when R was 4-Cl or 4-Br. Furthermore, when the compounds comprised moiety A1, their anti-inflammatory activities were significantly stronger than when the compounds comprised moiety A2. Moreover, the results signified that when the X of the C part was a carbon atom, the anti-inflammatory activities were significantly stronger than when X was a nitrogen atom. Initial anti-inflammatory screening and dose-dependent screening alluded that **13a** was the most potent derivative. Additionally, **13a** was able to inhibit LPS-induced activation of the NF-κB pathway, which, in turn, reduced the transcription of proinflammatory genes and the release of proinflammatory cytokines, thereby alleviating the LPS-induced inflammatory response. This promising derivative exerted an obvious protective effect on LPS-induced ALI mice and significantly reduced the levels of proinflammatory cytokines in serum and BALF. Furthermore, **13a** decreased the mRNA levels of some proinflammatory cytokines in the lung tissue, improved the histopathological changes in the lung tissue, and reduced macrophage infiltration. The protective effect of **13a** in ALI mice was close to that of DXMS and even surpassed DXMS in some aspects. Derivative **13a** also had an obvious protective effect on LPS-induced sepsis mice, slowing down death and improving weight loss. Thus, our findings signify that 4-oxo-*N*-phenyl-1,4-dihydroquinoline-3-carboxamide derivative **13a** is a promising candidate for the treatment of ALI and sepsis.

Table 2
PK Study of compound **13a** in Rats.

parameter	iv (1 mg/kg)	po (10 mg/kg)
$AUC_{(0-t)}$ (μg/L·h)	6316	22,922
T_{max} (h)		5.0
$T_{1/2}$ (h)	8.9	11.8
C_{max} (μg/L)	1362	1680
F (%)		36.3

4. Experimental

4.1. Chemical synthesis

Generally, all chemicals were of reagent grade and used without purification. The melting points of all compounds were determined using a Fisher–Johns melting apparatus, and the melting points were uncorrected. ^{1}H NMR and ^{13}C-HMR spectra were recorded on a 400 MHz spectrometer (Bruker Corporation, Switzerland) with TMS as an internal reference, and the chemical shifts were reported in parts per million. Electron-spray ionization mass spectra in positive mode data were obtained using a Bruker Esquire HCT spectrometer. All reactions were monitored using thin-layer chromatography (250 silica gel 60 F_{254} glass plates), and flash column chromatography purifications were performed using Merck silica gel 60 (230–400 mesh ASTM).

4.2. Procedure for the synthesis of intermediates 6a–6g

1-(2-chlorophenyl)ethan-1-one (1 g, 6.5 mmol) and NaH (1.3 g, 60%) were added to an anhydrous THF (30 mL) under an ice bath and stirred for 30 min. Later, dimethyl carbonate (3 g, 32 mmol) was added to the mixture and allowed to react for 3 h at 85 °C. Dilute hydrochloric acid was slowly added to the mixture, and the pH was adjusted to 3. Next, water (65 mL) was added to remove the water-soluble impurities, and dichloromethane (CH_2CL_2, 3 × 65 mL) was added for extraction. The organic phase was dried through anhydrous magnesium sulfate ($MgSO_4$) and concentration *in vacuo* to obtain intermediate **2** with a yield of 75%.

Intermediate **2** (20 mmol) and DMF-DMA (9 mL, 80 mmol) were dissolved in toluene (6 mL), and the mixture was refluxed at 120 °C for 2 h. Toluene was removed with an oil pump vacuum, and the residue was dissolved in CH_2CL_2 (150 mL). The organic phase was washed with water (3 × 40 mL) and saturated brine (80 mL) to remove the water-soluble impurities. Finally, the organic phase was dried over anhydrous sodium sulfate, and the solvent was removed *in vacuo* to get

intermediate **3** with a yield of 75%.

Intermediate **3** (10 mmol) and an appropriate amount of aniline (11 mmol) were dissolved in toluene (20 mL), and the mixture was reacted at 110 °C for 4 h to obtain intermediates **4a**–**4g**. Subsequently, Cs_2CO_3 (3.26 g 10 mmol) and K_2CO_3 (1.38 g 10 mmol) were added to the mixture, the temperature was increased to 150 °C, and the reaction was continued for 6 h Cs_2CO_3 was then removed via suction filtration, and the filtrate was concentrated *in vacuo* to obtain the crude products **5a**–**5g** with a yield of 60%–75%.

5a–**5g** (10 mmol) and NaOH (20 mmol) were dissolved in 1,4-dioxane/water (2 : 1), and the reaction system was heated to 100 °C for 2 h. Then, 1,4-dioxane was removed using an oil pump vacuum, saturated brine (20 mL) was added to dissolve the residue, and dilute hydrochloric acid was added to adjust the pH to 3. At this point, a large amount of precipitate was produced, which was collected using suction filtration and dried to obtain the crude products**.** Finally, the crude products were purified with silica gel chromatography using CH_2Cl_2 and MeOH in a ratio of 8:1 to derive the intermediates **6a**–**6g** with a yield of 65%–75%.

*4.2.1. 4-oxo-1-phenyl-1,4-dihydroquinoline-3-carboxylic acid (**6a**)*

Yellow power; yield: 63.1%. ^{1}H NMR (400 MHz, $CDCl_3$) δ 14.91 (s, 1H), 8.84 (s, 1H), 8.60 (d, J = 8.1 Hz, 1H), 7.73 (d, J = 8.4 Hz, 1H), 7.70 (s, 1H), 7.69 (d, J = 3.2 Hz, 2H), 7.61 (t, J = 7.6 Hz, 1H), 7.48 (d, J = 3.2 Hz, 1H), 7.47 (d, J = 2.5 Hz, 1H), 7.19 (d, J = 8.6 Hz, 1H).

*4.2.2. 1-(4-fluorophenyl)-4-oxo-1,4-dihydroquinoline-3-carboxylic acid (**6b**)*

Yellow power; yield: 66.5%. ^{1}H NMR (400 MHz, $CDCl_3$) δ 14.82 (s, 1H), 8.82 (s, 1H), 8.62 (d, J = 7.9 Hz, 1H), 7.73 (t, J = 7.9 Hz, 1H), 7.63 (t, J = 7.3 Hz, 1H), 7.49 (d, J = 4.8 Hz, 1H), 7.47 (d, J = 4.3 Hz, 1H), 7.41 (s, 1H), 7.38 (d, J = 8.4 Hz, 1H), 7.15 (d, J = 8.4 Hz, 1H).

*4.2.3. 1-(4-chloro-2-fluorophenyl)-4-oxo-1,4-dihydroquinoline-3-carboxylic acid (**6c**)*

Yellow power; yield: 70.3%. ^{1}H NMR (400 MHz, $CDCl_3$) δ 14.79 (s, 1H), 8.80 (s, 1H), 8.60 (d, J = 8.0 Hz, 1H), 7.74 (t, J = 7.7 Hz, 1H), 7.69 (s, 1H), 7.67 (s, 1H), 7.63 (t, J = 7.6 Hz, 1H), 7.45 (s, 1H), 7.43 (s, 1H), 7.17 (d, J = 8.5 Hz, 1H).

*4.2.4. 1-(4-bromophenyl)-4-oxo-1,4-dihydroquinoline-3-carboxylic acid (**6d**)*

Yellow power; yield: 60.9%. ^{1}H NMR (400 MHz, $CDCl_3$) δ 14.78 (s, 1H), 8.79 (s, 1H), 8.60 (d, J = 8.0 Hz, 1H), 7.85 (s, 1H), 7.83 (s, 1H), 7.74 (t, J = 7.8 Hz, 1H), 7.63 (t, J = 7.6 Hz, 1H), 7.38 (s, 1H), 7.36 (s, 1H), 7.17 (d, J = 8.6 Hz, 1H).

*4.2.5. 1-(4-chloro-2-fluorophenyl)-4-oxo-1,4-dihydroquinoline-3-carboxylic acid (**6e**)*

Yellow power; yield: 58.7%. ^{1}H NMR (400 MHz, $CDCl_3$) δ 14.68 (s, 1H), 8.75 (s, 1H), 8.61 (d, J = 7.9 Hz, 1H), 7.76 (t, J = 7.7 Hz, 1H), 7.66 (s, 1H), 7.64 (s, 1H), 7.62 (s, 1H), 7.41 (t, J = 8.0 Hz, 1H), 7.08 (d, J = 8.5 Hz, 1H).

*4.2.6. 1-(3-chloro-4-fluorophenyl)-4-oxo-1,4-dihydroquinoline-3-carboxylic acid (**6f**)*

Yellow power; yield: 55.1%. ^{1}H NMR (400 MHz, $CDCl_3$) δ 14.72 (s, 1H), 8.81 (s, 1H), 8.63 (d, J = 8.0 Hz, 1H), 7.78 (t, J = 7.6 Hz, 1H), 7.67 (d, J = 7.6 Hz, 1H), 7.63 (d, J = 5.5 Hz, 1H), 7.50 (t, J = 8.2 Hz, 1H), 7.43 (d, J = 7.4 Hz, 1H), 7.18 (d, J = 8.1 Hz, 1H).

*4.2.7. 4-oxo-1-(4-(trifluoromethoxy)phenyl)-1,4-dihydroquinoline-3-carboxylic acid (**6g**)*

Yellow power; yield: 68.1%. ^{1}H NMR (400 MHz, $CDCl_3$) δ 14.71 (s, 1H), 8.76 (s, 1H), 8.56 (d, J = 8.1 Hz, 1H), 7.71 (t, J = 7.8 Hz, 1H), 7.59 (t, J = 7.6 Hz, 1H), 7.53 (s, 1H), 7.51 (s, 1H), 7.51 (s, 1H), 7.49 (s, 1H), 7.12 (d, J = 8.6 Hz, 1H).

4.3. General procedure for the synthesis of intermediates 10a–10d

4-Chloro-6,7-dimethoxyquinoline (**7a**) or 4-chloro-6,7-dimethoxyquinazoline (**7b**) and 3-nitrophenol (**8a**) or 4-nitrophenol (**8b**) were dissolved in toluene (10 mL), NaI (0.1 mmol) was added as a catalyst, and Na_2CO_3 (20 mmol) was added to adjust the pH. The mixture was reacted at 130 °C overnight and spin-dried to obtain crude products **9a**–**9d** with a yield of 60%–70% Intermediates **9a**–**9d** (10 mmol) were dissolved in a mixed solution of water (5 mL) and ethanol (10 mL), following which reduced iron powder (20 mmol) and ammonium chloride (20 mmol) were added to the solution and allowed to react at 50 °C for 6 h. After the completion of the reaction, the inorganic residues were removed via filtration and the filtrate was dried *in vacuo* to obtain the crude product. Finally, the crude product was purified with silica gel chromatography using CH_2Cl_2 and MeOH in a ratio of 10:1 to acquire **10a**–**10d** with a yield of 60%–70%.

*4.3.1. 3-((6,7-dimethoxyquinolin-4-yl)oxy)aniline (**10a**)*

White power; yield: 59.7%. ^{1}H NMR (400 MHz, $CDCl_3$) δ 8.53 (d, J = 5.3 Hz, 1H), 7.57 (s, 1H), 7.45 (s, 1H), 7.25 (t, J = 8.0 Hz, 1H), 6.62 (d, J = 8.0 Hz, 1H), 6.60 (s, 1H), 6.58 (s, 1H), 6.53 (d, J = 2.1 Hz, 1H), 5.22 (s, 2H), 4.08 (d, J = 4.3 Hz, 6H).

*4.3.2. 3-((6,7-dimethoxyquinazolin-4-yl)oxy)aniline (**10b**)*

Yellow power; yield: 50.7%. ^{1}H NMR (400 MHz, $CDCl_3$) δ 8.67 (s, 1H), 7.57 (s, 1H), 7.34 (s, 1H), 7.31–7.26 (m, 1H), 6.66 (dd, J = 4.7, 2.1 Hz, 1H), 6.64 (d, J = 4.3 Hz, 1H), 6.61 (d, J = 2.0 Hz, 1H), 5.33 (s, 2H), 4.09 (s, 6H).

*4.3.3. 4-((6,7-dimethoxyquinolin-4-yl)oxy)aniline (**10c**)*

Yellow power; yield: 50.7%. ^{1}H NMR (400 MHz, DMSO-d_6) δ 8.44 (d, J = 5.2 Hz, 1H), 7.52 (s, 1H), 7.38 (s, 1H), 6.95 (s, 1H), 6.93 (s, 1H), 6.70 (s, 1H), 6.67 (s, 1H), 6.39 (d, J = 5.2 Hz, 1H), 5.17 (s, 2H), 3.95 (s, 6H).

*4.3.4. 4-((6,7-dimethoxyquinazolin-4-yl)oxy)aniline (**10d**)*

White power; yield: 68.1%. ^{1}H NMR (400 MHz, $CDCl_3$) δ 8.66 (s, 1H), 7.59 (s, 1H), 7.34 (s, 1H), 7.08 (s, 1H), 7.06 (s, 1H), 6.82 (s, 1H), 6.79 (s, 1H), 5.33 (s, 2H), 4.10 (s, 6H).

4.4. General procedure for the synthesis of the compounds 11a–11g, 12a–12g, 13a–13g, and 14a–14g

The corresponding amines **10a**–**10d** (1 mmol) and the acids **6a**–**6d** (1 mmol) were dissolved in DMF (6 mL), HATU (1 mmol) and DIPEA (1.2 mmol) were added to the mixture, and an acid–amine condensation reaction was performed at room temperature for 16 h. Next, ice water was added dropwise to the mixture. A large amount of solid was precipitated out, which was collected using suction filtration and dried to obtain the crude products. These products were then dissolved in ethyl acetate (10 mL). The organic phase was washed with water (3 × 20 mL) and saturated brine (40 mL) to remove DMF. Finally, the organic phase was concentrated i*n vacuo* and purified with silica gel chromatography using CH_2Cl_2 and MeOH in a ratio of 20:1 to obtain **11a**–**11g, 12a**–**12g, 13a**–**13g, and 14a**–**14g** as solids.

*4.4.1. N-(3-((6,7-dimethoxyquinolin-4-yl)oxy)phenyl)-4-oxo-1-phenyl-1,4-dihydroquinoline-3-carboxamide (**11a**)*

Yellow power; yield: 50.4%; m.p.: 215.7–217.1 °C. ^{1}H NMR (400 MHz, $CDCl_3$) δ 12.38 (s, 1H), 8.84 (s, 1H), 8.60 (d, J = 7.8 Hz, 1H), 8.57–8.50 (m, 1H), 7.89 (s, 1H), 7.69 (t, J = 7.4 Hz, 1H), 7.61 (s, 2H), 7.60 (d, J = 2.1 Hz, 1H), 7.58 (s, 1H), 7.55 (d, J = 5.5 Hz, 1H), 7.50 (d, J = 9.0 Hz, 1H), 7.47 (s, 1H), 7.46 (s, 1H), 7.43 (d, J = 6.9 Hz, 1H), 7.41–7.35 (m, 1H), 7.11 (d, J = 8.4 Hz, 1H), 6.99 (d, J = 9.2 Hz, 1H), 6.63 (d, J = 5.1 Hz, 1H), 4.09 (s, 6H). ^{13}C NMR (101 MHz, $CDCl_3$) δ

177.00, 163.11, 160.53, 154.97, 152.81, 149.48,148.95, 147.99, 146.86, 140.75, 140.58, 140.52, 133.00, 130.53 (2C), 130.32 (2C), 127.24 (2C), 127.13,126.93, 125.76, 118.15, 117.28, 116.31, 116.11, 113.26, 111.89, 107.80, 103.85, 99.64, 56.21,56.16. ESI-MS: *m/z* 544.2 $[M+H]^+$.

4.4.2. N-(3-((6,7-dimethoxyquinolin-4-yl)oxy)phenyl)-1-(4-fluorophenyl)-4-oxo-1,4-dihydroquinoline-3-carboxamide (**11b**)

Yellow power; yield: 55.9%; m.p.: 189.5–190.8 °C. ^{1}H NMR (400 MHz, $CDCl_3$) δ 12.45 (s, 1H), 8.88 (s, 1H), 8.62 (d, *J* = 7.9 Hz, 1H), 8.54 (d, *J* = 5.2 Hz, 1H), 7.90 (s, 1H), 7.67 (t, *J* = 7.2 Hz, 1H), 7.62 (s, 1H), 7.61–7.59 (m, 1H), 7.57 (d, *J* = 7.7 Hz, 1H), 7.49 (s, 1H), 7.48 (s, 1H), 7.47 (s, 1H), 7.46 (s, 1H), 7.37 (t, *J* = 8.3 Hz, 2H), 7.11 (d, *J* = 8.5 Hz, 1H), 6.99 (d, *J* = 8.0 Hz, 1H), 6.63 (d, *J* = 5.3 Hz, 1H), 4.09 (s, 6H). ESI-MS: *m/z* 562.2 $[M+H]^+$.

4.4.3. 1-(4-bromophenyl)-N-(3-((6,7-dimethoxyquinazolin-4-yl)oxy)phenyl)-4-oxo-1,4-dihydroquinoline-3-carboxamide (**11c**)

Yellow power; yield: 50.7%; m.p.: 226.0–227.1 °C. ^{1}H NMR (400 MHz, $CDCl_3$) δ 12.43 (s, 1H), 8.87 (s, 1H), 8.61 (d, *J* = 8.0 Hz, 1H), 8.54 (d, *J* = 5.2 Hz, 1H), 7.89 (s, 1H), 7.67 (d, *J* = 8.6 Hz, 2H), 7.64 (s, 1H), 7.61 (s, 2H), 7.58 (d, *J* = 8.2 Hz, 1H), 7.48 (d, *J* = 7.9 Hz, 2H), 7.44 (s, 1H), 7.42 (s, 1H), 7.13 (d, *J* = 8.4 Hz, 1H), 6.99 (d, *J* = 8.0 Hz, 1H), 6.62 (d, *J* = 5.3 Hz, 1H), 4.09 (s, 6H). ESI-MS: *m/z* 578.2 $[M+H]^+$.

4.4.4. 1-(4-bromophenyl)-N-(3-((6,7-dimethoxyquinolin-4-yl)oxy)phenyl)-4-oxo-1,4-dihydroquinoline-3-carboxamide (**11d**)

Yellow power; yield: 52.9%; m.p.: 205.0–206.8 °C. ^{1}H NMR (400 MHz, $CDCl_3$) δ 12.36 (s, 1H), 8.81 (s, 1H), 8.61 (d, *J* = 8.0 Hz, 1H), 8.54 (d, *J* = 5.3 Hz, 1H), 7.89 (s, 1H), 7.69 (dd, *J* = 11.5, 4.0 Hz, 1H), 7.65 (d, *J* = 7.1 Hz, 1H), 7.63 (s, 1H), 7.61 (s, 2H), 7.59 (s, 1H), 7.59–7.54 (m, 1H), 7.48 (d, *J* = 5.9 Hz, 1H), 7.45 (s, 1H), 7.41 (t, *J* = 8.2 Hz, 1H), 7.04 (d, *J* = 8.5 Hz, 1H), 6.99 (d, *J* = 8.1 Hz, 1H), 6.63 (d, *J* = 5.3 Hz, 1H), 4.09 (s, 6H). ESI-MS: *m/z* 622.1 $[M+H]^+$.

4.4.5. 1-(4-bromo-2-fluorophenyl)-N-(3-((6,7-dimethoxyquinolin-4-yl)oxy)phenyl)-4-oxo-1,4-dihydroquinolne-3-carboxamide (**11e**)

Yellow power; yield: 53.3%; m.p.: 225.1–227.5 °C. ^{1}H NMR (400 MHz, $CDCl_3$) δ 12.38 (s, 1H), 8.81 (s, 1H), 8.61 (dd, *J* = 8.1, 1.2 Hz, 1H), 8.54 (d, *J* = 5.4 Hz, 1H), 7.92 (t, *J* = 2.0 Hz, 1H), 7.70 (dd, *J* = 8.6, 1.5 Hz, 1H), 7.66–7.63 (m, 1H), 7.62 (s, 1H), 7.61 (d, *J* = 3.0 Hz, 1H), 7.59 (s, 1H), 7.59 (s, 1H), 7.57 (d, *J* = 4.2 Hz, 1H), 7.48 (t, *J* = 8.1 Hz, 1H), 7.41 (dd, *J* = 11.1, 5.3 Hz, 1H), 7.04 (d, *J* = 8.5 Hz, 1H), 6.99 (dd, *J* = 7.7, 1.9 Hz, 1H), 6.65 (d, *J* = 5.4 Hz, 1H), 4.10 (d, *J* = 3.8 Hz, 6H). ESI-MS: *m/z* 640.1 $[M+H]^+$.

4.4.6. 1-(3-chloro-4-fluorophenyl)-N-(3-((6,7-dimethoxyquinolin-4-yl)oxy)phenyl)-4-oxo-1,4-dihydroquinoine-3-carboxamide (**11f**)

Brown power; yield: 56.3%; m.p.: 225.1–227.5 °C. ^{1}H NMR (400 MHz, CDCl3) δ 12.41 (s, 1H), 8.88 (s, 1H), 8.62 (d, *J* = 8.0 Hz, 1H), 8.54 (d, *J* = 5.3 Hz, 1H), 7.88 (s, 1H), 7.68 (t, *J* = 7.2 Hz, 1H), 7.61 (d, *J* = 4.0 Hz, 2H), 7.57 (d, *J* = 7.7 Hz, 1H), 7.54 (s, 3H), 7.50–7.44 (m, 2H), 7.12 (d, *J* = 8.5 Hz, 1H), 6.99 (d, *J* = 6.9 Hz, 1H), 6.62 (d, *J* = 5.3 Hz, 1H), 4.09 (s, 6H). ESI-MS: *m/z* 596.1 $[M+H]^+$.

4.4.7. N-(3-((6,7-dimethoxyquinolin-4-yl)oxy)phenyl)-4-oxo-1-(4-(trifluoromethoxy)phenyl)-1,4-dihydroquinoline-3-carboxamide (**11g**)

Yellow power; yield: 48.6%; m.p.: 182.2–184.1 °C. ^{1}H NMR (400 MHz, $CDCl_3$) δ 12.50 (s, 1H), 8.92 (s, 1H), 8.69 (s, 1H), 8.62 (d, *J* = 8.2 Hz, 1H), 7.99 (s, 1H), 7.70 (d, *J* = 4.8 Hz, 1H), 7.67 (d, *J* = 3.5 Hz, 1H), 7.66 (s, 1H), 7.65 (s, 1H), 7.63 (s, 1H), 7.62 (s, 1H), 7.56 (t, *J* = 7.4 Hz, 1H), 7.51 (d, *J* = 8.3 Hz, 1H), 7.49 (d, *J* = 5.3 Hz, 1H), 7.47 (t, *J* = 4.2 Hz, 1H), 7.36 (s, 1H), 7.16 (d, *J* = 8.4 Hz, 1H), 7.08 (d, *J* = 9.0 Hz, 1H), 4.11 (s, 6H). ^{13}C NMR (101 MHz, $CDCl_3$) δ 177.07, 163.06, 160.87, 154.68, 153.08, 150.12, 149.58, 148.36, 147.84, 146.20, 140.51, 140.21, 138.57, 133.39, 130.42, 129.02 (2C), 126.91 (2C), 126.01, 122.76 (2C), 117.84, 117.52, 116.41, 116.26, 113.32, 111.96, 111.88, 106.74, 103.64, 99.59, 56.10, 56.05. ESI-MS: *m/z* 628.2 $[M+H]^+$.

4.4.8. N-(3-((6,7-dimethoxyquinazolin-4-yl)oxy)phenyl)-4-oxo-1-phenyl-1,4-dihydroquinoline-3-carboxamide (**12a**)

White power; yield: 37.8%; m.p.: 246.4–248.0 °C. ^{1}H NMR (400 MHz, $CDCl_3$) δ 12.50 (s, 1H), 8.92 (s, 1H), 8.69 (s, 1H), 8.62 (d, *J* = 7.7 Hz, 1H), 7.99 (s, 1H), 7.68 (d, *J* = 6.3 Hz, 1H), 7.66 (s, 1H), 7.66 (s, 1H), 7.65 (s, 1H), 7.63 (s, 1H), 7.62 (s, 1H), 7.56 (t, *J* = 7.4 Hz, 1H), 7.51 (d, *J* = 8.3 Hz, 1H), 7.49 (s, 1H), 7.48 (d, *J* = 2.5 Hz, 1H), 7.36 (s, 1H), 7.16 (d, *J* = 8.4 Hz, 1H), 7.08 (d, *J* = 7.9 Hz, 1H), 4.11 (s, 6H). ESI-MS: *m/z* 567.2 $[M+Na]^+$.

4.4.9. N-(3-((6,7-dimethoxyquinazolin-4-yl)oxy)phenyl)-1-(4-fluorophenyl)-4-oxo-1,4-dihydroquinoline-3-carboxamide (**12b**)

Yellow power; yiled: 32.6%; m.p.: 260.1–261.4 °C ^{1} H NMR (400 MHz, $CDCl_3$) δ 12.42 (s, 1H), 8.84 (s, 1H), 8.67 (s, 1H), 8.58 (d, *J* = 8.0 Hz, 1H), 7.96 (s, 1H), 7.63 (t, *J* = 7.2 Hz, 1H), 7.60 (d, *J* = 8.2 Hz, 1H), 7.59 (s, 1H), 7.54 (t, *J* = 7.5 Hz, 1H), 7.48 (d, *J* = 8.3 Hz, 1H), 7.46–7.44 (m, 1H), 7.43 (s, 1H), 7.41 (s, 1H), 7.35 (s, 1H), 7.32 (d, *J* = 8.6 Hz, 1H), 7.07 (d, *J* = 8.7 Hz, 1H), 7.04 (d, *J* = 8.2 Hz, 1H), 4.08 (s, 6H). ESI-MS: *m/z* 563.2 $[M+H]^+$.

4.4.10. 1-(4-chlorophenyl)-N-(3-((6,7-dimethoxyquinazolin-4-yl)oxy)phenyl)-4-oxo-1,4-dihydroquinoline-3-carboxamide (**12c**)

Yellow solid; yiled: 31.5%; m.p.: 273.4–274.8 °C. ^{1}H NMR (400 MHz, $CDCl_3$) δ 12.49 (s, 1H), 8.87 (s, 1H), 8.74 (s, 1H), 8.62 (d, *J* = 7.5 Hz, 1H), 8.03 (s, 1H), 7.83 (s, 1H), 7.81 (s, 1H), 7.68 (t, *J* = 7.9 Hz, 1H), 7.64 (s, 1H), 7.62 (s, 1H), 7.61 (d, *J* = 3.9 Hz, 1H), 7.57 (d, *J* = 7.2 Hz, 1H), 7.52 (t, *J* = 8.1 Hz, 1H), 7.39 (s, 1H), 7.37 (s, 1H), 7.14 (d, *J* = 8.4 Hz, 1H), 7.07 (d, *J* = 9.3 Hz, 1H), 4.14 (d, *J* = 7.8 Hz, 6H). ^{13}C NMR (101 MHz, $CDCl_3$) δ 176.96, 165.91, 162.86, 156.65, 152.66, 151.95, 150.74, 147.73, 147.11, 140.58, 140.18, 138.92, 136.50, 133.18, 130.81 (2C), 129.96, 128.69 (2C), 127.10 (2C), 125.91, 117.97, 117.82, 117.07, 113.98, 112.16, 110.68, 105.40, 101.26, 56.75, 56.52. ESI-MS: *m/z* 579.3 $[M+H]^+$.

4.4.11. 1-(4-bromophenyl)-N-(3-((6,7-dimethoxyquinazolin-4-yl)oxy)phenyl)-4-oxo-1,4-dihydroquinoline-3-carboxamide (**12d**)

Yellow solid; yiled: 33.5%; m.p.: 280.1–281.7 °C ^{1} H NMR (400 MHz, $CDCl_3$) δ 12.45 (s, 1H), 8.86 (s, 1H), 8.72 (s, 1H), 8.61 (d, *J* = 7.9 Hz, 1H), 8.00 (s, 1H), 7.82 (s, 1H), 7.80 (s, 1H), 7.67 (t, *J* = 7.7 Hz, 1H), 7.63 (s, 1H), 7.61 (s, 1H), 7.58 (d, *J* = 7.7 Hz, 1H), 7.54 (d, *J* = 12.3 Hz, 1H), 7.49 (d, *J* = 8.1 Hz, 1H), 7.38 (s, 1H), 7.36 (s, 1H), 7.13 (d, *J* = 8.4 Hz, 1H), 7.07 (d, *J* = 7.9 Hz, 1H), 4.12 (d, *J* = 4.5 Hz, 6H). ESI-MS: *m/z* 623.1 $[M+H]^+$.

4.4.12. 1-(4-bromo-2-fluorophenyl)-N-(3-((6,7-dimethoxyquinazolin-4-yl)oxy)phenyl)-4-oxo-1,4-dihydroquinoline-3-carboxamide (**12e**)

White solid; yiled: 34.7%; m.p.: 217.4–218.6 °C. ^{1}H NMR (400 MHz, $CDCl_3$) δ 12.36 (s, 1H), 8.81 (s, 1H), 8.69 (s, 1H), 8.62 (d, *J* = 8.0 Hz, 1H), 7.97 (s, 1H), 7.69 (t, *J* = 7.2 Hz, 1H), 7.64 (s, 1H), 7.61 (d, *J* = 6.3 Hz, 3H), 7.57 (d, *J* = 7.2 Hz, 1H), 7.50 (t, *J* = 8.1 Hz, 1H), 7.42 (t, *J* = 8.2 Hz, 1H), 7.36 (s, 1H), 7.09 (d, *J* = 7.7 Hz, 1H), 7.04 (d, *J* = 8.5 Hz, 1H), 4.11 (s, 6H). ^{13}C NMR (101 MHz, $CDCl_3$) δ 177.12, 165.42, 162.51, 158.66, 155.82, 153.07, 152.93, 150.16, 149.33, 147.89, 140.15, 140.00, 133.46, 130.36, 129.88, 129.40, 127.17, 127.02, 126.00, 125.34,121.50, 121.28, 117.73,117.33, 117.05, 114.16, 112.84, 110.83, 106.80, 101.17, 56.41 (2C). ESI-MS: *m/z* 641.1 $[M+H]^+$.

4.4.13. 1-(3-chloro-4-fluorophenyl)-N-(3-((6,7-dimethoxyquinazolin-4-yl)oxy)phenyl)-4-oxo-1,4-dihydroquinoline-3-carboxamide (**12f**)

White solid; yiled: 37.7%; m.p.: 265.1–267.0 °C. ^{1}H NMR (400 MHz, $CDCl_3$) δ 12.37 (s, 1H), 8.85 (s, 1H), 8.68 (s, 1H), 8.61 (d, *J* = 7.1 Hz, 1H), 7.96 (s, 1H), 7.69 (t, *J* = 7.1 Hz, 1H), 7.63 (s, 1H), 7.61 (s, 1H), 7.60 (s, 1H), 7.57 (d, *J* = 7.7 Hz, 1H), 7.50 (t, *J* = 8.1 Hz, 1H), 7.45 (d, *J* = 8.1

Hz, 1H), 7.42 (d, J = 2.5 Hz, 1H), 7.36 (s, 1H), 7.12 (s, 1H), 7.09 (d, J = 9.2 Hz, 1H), 4.11 (d, J = 1.3 Hz, 6H). ^{13}C NMR (101 MHz, $CDCl_3$) δ 176.91, 165.44, 162.59, 155.85, 153.03, 152.94, 150.18, 149.32, 147.64, 140.49, 140.00, 136.84, 133.31, 130.06, 129.89, 127.50, 127.43, 127.18, 127.02, 125.99, 118.52, 118.29, 117.71, 117.59, 117.33, 114.14, 112.34, 110.82, 106.78, 101.16, 56.42, 56.41. ESI-MS: *m/z* 597.2 [M+H] $^+$.

4.4.14. N-(3-((6,7-dimethoxyquinazolin-4-yl)oxy)phenyl)-4-oxo-1-(4-(trifluoromethoxy)phenyl)-1,4-dihydroquinoline-3-carboxamide (12g)

White solid; yiled: 35.7%; m.p.: 273.1–274.0 °C. ^{1}H NMR (400 MHz, $CDCl_3$) δ 12.41 (s, 1H), 8.88 (s, 1H), 8.69 (s, 1H), 8.62 (d, J = 7.9 Hz, 1H), 7.97 (s, 1H), 7.68 (t, J = 7.2 Hz, 1H), 7.64 (s, 1H), 7.62 (s, 1H), 7.59 (d, J = 7.5 Hz, 1H), 7.57 (d, J = 2.9 Hz, 1H), 7.55 (s, 1H), 7.53 (d, J = 6.7 Hz, 2H), 7.49 (d, J = 8.1 Hz, 1H), 7.36 (s, 1H), 7.12 (d, J = 8.5 Hz, 1H), 7.09 (d, J = 8.1 Hz, 1H), 4.11 (d, J = 0.9 Hz, 6H). ESI-MS: *m/z* 651.2 [M+Na] $^+$.

4.4.15. N-(4-((6,7-dimethoxyquinolin-4-yl)oxy)phenyl)-4-oxo-1-phenyl-1,4-dihydroquinoline-3-carboxamide (13a)

Yellow solid; yiled: 55.7%; m.p.: 225.1–226.6 °C. ^{1}H NMR (400 MHz, $CDCl_3$) δ 12.47 (s, 1H), 8.97 (s, 1H), 8.64 (d, J = 7.8 Hz, 1H), 8.54 (s, 1H), 7.95 (s, 1H), 7.93 (s, 1H), 7.69 (s, 1H), 7.68 (s, 2H), 7.64 (d, J = 7.8 Hz, 1H), 7.60 (s, 1H), 7.57 (d, J = 7.5 Hz, 1H), 7.53 (s, 1H), 7.51 (s, 1H), 7.49 (s, 1H), 7.24 (s, 1H), 7.22 (s, 1H), 7.17 (d, J = 8.5 Hz, 1H), 6.57 (d, J = 5.0 Hz, 1H), 4.10 (s, 6H). ^{13}C NMR (101 MHz, $CDCl_3$) δ 177.03, 163.47, 163.08, 154.72, 150.59, 149.06, 147.95, 144.86, 140.77, 142.46, 140.46, 137.18, 133.06, 130.55 (2C), 130.36, 127.26 (2C), 127.09, 126.89, 125.80, 122.30 (2C), 121.57 (2C), 118.19, 116.08, 111.84, 104.31, 102.91, 99.76, 56.74, 56.42. ESI-MS: *m/z* 544.2 [M+H] $^+$.

4.4.16. N-(4-((6,7-dimethoxyquinolin-4-yl)oxy)phenyl)-1-(4-fluorophenyl)-4-oxo-1,4-dihydroquinoline-3-carboxamide (13b)

Yellow solid; yiled: 59.3%; m.p.: 256.9–258.8 °C. ^{1}H NMR (400 MHz, $CDCl_3$) δ 12.40 (s, 1H), 8.93 (d, J = 3.1 Hz, 1H), 8.63 (d, J = 8.0 Hz, 1H), 8.52 (d, J = 5.1 Hz, 1H), 7.93 (s, 1H), 7.91 (d, J = 2.9 Hz, 1H), 7.68 (t, J = 7.7 Hz, 1H), 7.61 (d, J = 3.0 Hz, 1H), 7.57 (d, J = 8.1 Hz, 1H), 7.53–7.45 (m, 3H), 7.38 (t, J = 9.7 Hz, 2H), 7.24 (d, J = 3.0 Hz, 1H), 7.22 (d, J = 3.0 Hz, 1H), 7.12 (d, J = 10.4 Hz, 1H), 6.55 (s, 1H), 4.09 (s, 6H). ^{13}C NMR (101 MHz, $CDCl_3$) δ 176.98, 162.79, 161.47, 153.22, 149.96, 149.71, 148.00, 147.90, 145.84, 140.81, 136.49, 136.46, 133.12, 130.94, 129.38, 129.29, 128.85, 127.08, 127.01, 125.82, 122.13 (2C), 121.61 (2C), 117.88, 117.76, 117.53, 112.10, 107.02, 103.26, 99.61, 56.26 (2C). ESI-MS: *m/z* 562.2 [M+H] $^+$.

4.4.17. 1-(4-chlorophenyl)-N-(4-((6,7-dimethoxyquinolin-4-yl)oxy)phenyl)-4-oxo-1,4-dihydroquinoline-3-carboxamide (13c)

Yellow solid; yiled: 55.2%; m.p.: 249.1–250.2 °C. ^{1}H NMR (400 MHz, $CDCl_3$) δ 12.41 (s, 1H), 8.93 (s, 1H), 8.64 (dd, J = 8.1, 1.4 Hz, 1H), 8.53 (d, J = 5.4 Hz, 1H), 7.96–7.94 (m, 1H), 7.93–7.91 (m, 1H), 7.71–7.69 (m, 1H), 7.68 (s, 1H), 7.66 (d, J = 2.8 Hz, 1H), 7.63 (s, 1H), 7.62–7.56 (m, 1H), 7.54 (s, 1H), 7.47 (d, J = 1.9 Hz, 1H), 7.46–7.44 (m, 1H), 7.26–7.24 (m, 1H), 7.23 (s, 1H), 7.15 (d, J = 8.5 Hz, 1H), 6.58 (d, J = 5.4 Hz, 1H), 4.10 (s, 6H). ^{13}C NMR (101 MHz, $CDCl_3$) δ 177.01, 162.73, 160.91, 152.81, 150.25, 149.48, 148.94, 147.68, 146.84, 140.60, 138.94, 136.51, 136.21, 133.15, 130.82 (2C), 128.72 (2C), 127.09, 125.88, 122.12 (2C), 121.64 (2C), 117.82 (2C), 116.12, 112.28, 107.83, 103.38, 99.59, 56.21, 56.16. ESI-MS: *m/z* 578.2 [M+H] $^+$.

4.4.18. 1-(4-bromophenyl)-N-(4-((6,7-dimethoxyquinolin-4-yl)oxy)phenyl)-4-oxo-1,4-dihydroquinoline-3-carboxamide (13d)

White solid; yiled: 58.8%; m.p.: 257.1–259.0 °C ^{1} H NMR (400 MHz, $CDCl_3$) δ 12.38 (s, 1H), 8.92 (s, 1H), 8.64 (d, J = 8.0 Hz, 1H), 8.53 (d, J = 5.2 Hz, 1H), 7.93 (s, 1H), 7.91 (s, 1H), 7.84 (s, 1H), 7.82 (s, 1H), 7.68 (t, J = 7.8 Hz, 1H), 7.62 (s, 1H), 7.58 (d, J = 7.2 Hz, 1H), 7.47 (s, 1H), 7.40 (s, 1H), 7.38 (s, 1H), 7.24 (s, 1H), 7.22 (s, 1H), 7.15 (d, J = 8.5 Hz, 1H), 6.55 (d, J = 5.3 Hz, 1H), 4.09 (d, J = 1.8 Hz, 6H). ESI-MS: *m/z* 622.1 [M+H] $^+$.

4.4.19. 1-(4-bromo-2-fluorophenyl)-N-(4-((6,7-dimethoxyquinolin-4-yl)oxy)phenyl)-4-oxo-1,4-dihydroquinoline-3-carboxamide (13e)

Yellow solid; yiled: 60.3%; m.p.: 248.5–250.1 °C ^{1} H NMR (400 MHz, $CDCl_3$) δ 12.31 (s, 1H), 8.86 (s, 1H), 8.63 (d, J = 8.0 Hz, 1H), 8.53 (d, J = 5.3 Hz, 1H), 7.93 (s, 1H), 7.91 (s, 1H), 7.70 (t, J = 7.3 Hz, 1H), 7.65 (s, 1H), 7.63 (s, 1H), 7.61 (s, 1H), 7.58 (d, J = 7.8 Hz, 1H), 7.46 (s, 1H), 7.43 (d, J = 8.5 Hz, 1H), 7.24 (s, 1H), 7.22 (s, 1H), 7.06 (d, J = 8.5 Hz, 1H), 6.54 (d, J = 5.3 Hz, 1H), 4.09 (d, J = 2.0 Hz, 6H). ESI-MS: *m/z* 662.0 [M+Na] $^+$.

4.4.20. 1-(3-chloro-4-fluorophenyl)-N-(4-((6,7-dimethoxyquinolin-4-yl)oxy)phenyl)-4-oxo-1,4-dihydroquinoline-3-carboxamide (13f)

Yellow solid; yiled: 54.5%; m.p.: 210.1–211.2 °C. ^{1}H NMR (400 MHz, $CDCl_3$) δ 12.33 (s, 1H), 8.90 (s, 1H), 8.63 (d, J = 7.4 Hz, 1H), 8.52 (d, J = 5.3 Hz, 1H), 7.93 (s, 1H), 7.90 (s, 1H), 7.70 (t, J = 7.2 Hz, 1H), 7.63 (d, J = 6.3 Hz, 1H), 7.61 (s, 1H), 7.59 (d, J = 7.5 Hz, 1H), 7.49 (d, J = 8.6 Hz, 1H), 7.45 (d, J = 7.6 Hz, 2H), 7.24 (s, 1H), 7.22 (s, 1H), 7.13 (d, J = 8.5 Hz, 1H), 6.54 (d, J = 5.3 Hz, 1H), 4.09 (d, J = 2.1 Hz, 6H). ESI-MS: *m/z* 596.2 [M+H] $^+$.

4.4.21. N-(4-((6,7-dimethoxyquinolin-4-yl)oxy)phenyl)-4-oxo-1-(4-(trifluoromethoxy)phenyl)-1,4-dihydroquinoline-3-carboxamide (13g)

Yellow solid; yiled: 57.1%; m.p.: 230.5–232.0 °C. ^{1}H NMR (400 MHz, $CDCl_3$) δ 12.40 (s, 1H), 8.93 (s, 1H), 8.65 (d, J = 8.0 Hz, 1H), 8.53 (d, J = 5.4 Hz, 1H), 7.96 (s, 1H), 7.93 (s, 1H), 7.71 (t, J = 7.8 Hz, 1H), 7.63 (s, 1H), 7.62 (s, 1H), 7.59 (d, J = 2.7 Hz, 1H), 7.58 (s, 1H), 7.57 (s, 1H), 7.56 (s, 1H), 7.54 (s, 1H), 7.25 (s, 1H), 7.23 (s, 1H), 7.15 (d, J = 8.5 Hz, 1H), 6.59 (d, J = 5.5 Hz, 1H), 4.11 (s, 6H). ESI-MS: *m/z* 628.2 [M+H] $^+$.

4.4.22. N-(4-((6,7-dimethoxyquinazolin-4-yl)oxy)phenyl)-4-oxo-1-phenyl-1,4-dihydroquinoline-3-carboxamide (14a)

Yellow solid; yiled: 40.5%; m.p.: 246.8–247.8 °C. ^{1}H NMR (400 MHz, $CDCl_3$) δ 12.47 (s, 1H), 8.97 (s, 1H), 8.72 (s, 1H), 8.64 (d, J = 7.9 Hz, 1H), 7.98 (s, 1H), 7.97 (s, 1H), 7.67 (s, 3H), 7.64 (s, 1H), 7.63 (d, J = 2.5 Hz, 1H), 7.61–7.54 (m, 2H), 7.50 (d, J = 4.2 Hz, 1H), 7.49–7.46 (m, 1H), 7.30 (s, 1H), 7.28–7.26 (m, 1H), 7.17 (d, J = 7.0 Hz, 1H), 4.12 (d, J = 3.0 Hz, 6H). ESI-MS: *m/z* 545.2 [M+H] $^+$.

4.4.23. N-(4-((6,7-dimethoxyquinazolin-4-yl)oxy)phenyl)-1-(4-fluorophenyl)-4-oxo-1,4-dihydroquinoline-3-carboxamide (14b)

White solid; yield: 44.3%; m.p.: 248.0–250.0 °C. ^{1}H NMR (400 MHz, $CDCl_3$) δ12.40 (s, 1H), 8.93 (s, 1H), 8.69 (s, 1H), 8.64 (d, J = 8.1 Hz, 1H), 7.97 (s, 1H), 7.95 (s, 1H), 7.67 (t, J = 7.6 Hz, 1H), 7.62 (s, 1H), 7.58 (t, J = 7.4 Hz, 1H), 7.50 (dd, J = 7.3, 3.6 Hz, 2H), 7.42 (d, J = 0.7 Hz, 1H), 7.40 (d, J = 2.0 Hz, 1H), 7.38 (s, 1H), 7.30 (s, 1H), 7.29–7.27 (m, 1H), 7.12 (d, J = 8.5 Hz, 1H), 4.11 (s, 6H). ESI-MS: *m/z* 585.2 [M+Na] $^+$.

4.4.24. 1-(4-chlorophenyl)-N-(4-((6,7-dimethoxyquinazolin-4-yl)oxy)phenyl)-4-oxo-1,4-dihydroquinoline-3-carboxamide (14c)

Yellow solid; yiled: 48.1%; m.p.: 305.1–306.5 °C. ^{1}H NMR (400 MHz, $CDCl_3$) δ 12.37 (s, 1H), 8.92 (d, J = 2.9 Hz, 1H), 8.67 (d, J = 2.7 Hz, 1H), 8.63 (d, J = 9.5 Hz, 1H), 7.96 (s, 1H), 7.94 (s, 1H), 7.67 (s, 1H), 7.66 (s, 1H), 7.61 (s, 1H), 7.59 (d, J = 8.5 Hz, 1H), 7.56 (d, J = 7.6 Hz, 1H), 7.46 (d, J = 2.7 Hz, 1H), 7.44 (d, J = 2.6 Hz, 1H), 7.36 (d, J = 2.8 Hz, 1H), 7.30 (s, 1H), 7.28–7.26 (m, 1H), 7.13 (dd, J = 8.5, 2.0 Hz, 1H), 4.10 (s, 6H). ESI-MS: *m/z* 579.3 [M+H] $^+$.

4.4.25. 1-(4-bromophenyl)-N-(4-((6,7-dimethoxyquinazolin-4-yl)oxy)phenyl)-4-oxo-1,4-dihydroquinoline-3-carboxamide (14d)

Yellow solid; yiled: 46.6%; m.p.: 307.1–308.5 °C. ^{1}H NMR (400 MHz, $CDCl_3$) δ 12.38 (s, 1H), 8.93 (s, 1H), 8.68 (s, 1H), 8.64 (d, J = 8.0 Hz,

1H), 7.97 (s, 1H), 7.95 (s, 1H), 7.84 (s, 1H), 7.82 (s, 1H), 7.68 (t, $J = 7.8$ Hz, 1H), 7.62 (s, 1H), 7.59 (t, $J = 7.4$ Hz, 1H), 7.41 (s, 1H), 7.38 (s, 1H), 7.37 (s, 1H), 7.31 (s, 1H), 7.29 (s, 1H), 7.14 (d, $J = 8.4$ Hz, 1H), 4.11 (d, $J = 3.7$ Hz, 6H). ^{13}C NMR (101 MHz, $CDCl_3$) δ 176.98, 165.65, 162.59, 155.83, 153.05, 150.17, 149.28, 148.34, 147.60, 140.52, 139.50, 136.53, 133.80 (2C), 133.10, 129.00 (2C), 127.12, 127.09, 125.83, 124.46, 122.33 (2C), 121.60 (2C), 117.78, 112.37, 110.76, 106.82, 101.13, 56.43 (2C). ESI-MS: *m/z* 623.1 $[M+H]^+$.

4.4.26. 1-(4-bromo-2-fluorophenyl)-N-(4-((6,7-dimethoxyquinazolin-4-yl)oxy)phenyl)-4-oxo-1,4-dihydroquinoline-3-carboxamide (**14e**)

Yellow solid; yiled: 49.5%; m.p.: 251.3–252.7 °C. ^{1}H NMR (400 MHz, $CDCl_3$) δ 12.34 (s, 1H), 8.86 (s, 1H), 8.76–8.69 (m, 1H), 8.64 (d, $J = 7.9$ Hz, 1H), 7.98 (s, 1H), 7.96 (s, 1H), 7.71 (t, $J = 7.8$ Hz, 1H), 7.66 (s, 1H), 7.63 (s, 2H), 7.61 (d, $J = 8.0$ Hz, 1H), 7.58 (s, 1H), 7.44 (t, $J = 8.1$ Hz, 1H), 7.31 (s, 1H), 7.29 (s, 1H), 7.06 (d, $J = 8.4$ Hz, 1H), 4.13 (d, $J = 3.6$ Hz, 6H). ESI-MS: *m/z* 641.1 $[M+H]^+$.

4.4.27. 1-(3-chloro-4-fluorophenyl)-N-(4-((6,7-dimethoxyquinazolin-4-yl)oxy)phenyl)-4-oxo-1,4-dihydroquinoline-3-carboxamide (**14f**)

Yellow solid; yiled: 43.3%; m.p.: 251.1–216.3 °C. ^{1}H NMR (400 MHz, $CDCl_3$) δ 12.32 (s, 1H), 8.90 (s, 1H), 8.68 (s, 1H), 8.64 (d, $J = 8.0$ Hz, 1H), 7.96 (s, 1H), 7.94 (s, 1H), 7.70 (t, $J = 7.8$ Hz, 1H), 7.64 (s, 1H), 7.62 (s, 1H), 7.59 (d, $J = 7.7$ Hz, 1H), 7.51–7.45 (m, 1H), 7.45–7.41 (m, 1H), 7.37 (s, 1H), 7.31 (s, 1H), 7.29 (s, 1H), 7.13 (d, $J = 8.5$ Hz, 1H), 4.11 (d, $J = 3.9$ Hz, 6H). ESI-MS: *m/z* 597.2 $[M+H]^+$.

4.4.28. N-(4-((6,7-dimethoxyquinazolin-4-yl)oxy)phenyl)-4-oxo-1-(4-(trifluoromethoxy)phenyl)-1,4-dihydroquinoline-3-carboxamide (**14g**)

White solid; yiled: 42.9%; m.p.: 279.1–280.0 °C. ^{1}H NMR (400 MHz, $CDCl_3$) δ 12.37 (s, 1H), 8.93 (s, 1H), 8.69 (s, 1H), 8.64 (d, $J = 8.0$ Hz, 1H), 7.96 (d, $J = 4.7$ Hz, 1H), 7.95 (s, 1H), 7.69 (t, $J = 7.8$ Hz, 1H), 7.61 (s, 1H), 7.59 (s, 1H), 7.57 (s, 1H), 7.57 (s, 1H), 7.55 (s, 1H), 7.53 (s, 1H), 7.41 (s, 1H), 7.31 (s, 1H), 7.29 (s, 1H), 7.14 (d, $J = 8.5$ Hz, 1H), 4.12 (s, 6H). ^{13}C NMR (101 MHz, $CDCl_3$) δ 176.99, 165.65, 162.55, 155.83, 153.04, 150.17,150.13, 150.11, 149.30, 148.36, 147.70, 140.58, 138.79, 136.50, 133.16, 129.17 (2C), 127.12, 125.87, 122.78 (2C), 122.34 (2C), 121.60 (2C), 119.07, 117.72, 112.42, 110.76, 106.82, 101.12, 56.42 (2C). ESI-MS: *m/z* 629.2 $[M+H]^+$.

4.5. Reagents

The chemicals and LPS were procured from Sigma (Sigma, St. Louis, MO, USA). IL-6 and TNF-α ELISA kits were purchased from EBioscience (eBioScience, San Diego, CA, USA). TRIzol, gene primers, and the one-step M-MLV and Platinum SYBR Green qPCR SuperMix-UDG kit were obtained from Invitrogen (Invitrogen, Carlsbad, CA, USA). Chemiluminescence EMSA kit, ECL detection reagent, cellular NF-κB p65 translocation kit, and hematoxylin and eosin kit were sourced from Beyotime Biotechnology (Beyotime Biotech, Nantong, China). Anti-GAPDH, anti-IκB-α, anti-p65, anti-p-p65 and anti-F4/80 were obtained from Cell Signaling Technology (Danvers, MA, USA).

4.6. Cells and animals

J774A.1, THP-1 and LX-2 cells were obtained from Procell Life Science &Technology Co., Ltd. (Wuhan, China) and cultured in a DMEM medium containing 10% FBS at 37 °C with 5% CO_2. Six-week-old male C57BL/6 mice were purchased from GemPharmatech Co, Ltd (NanJing, China). All animal experiments conformed to the NIH guidelines, and all experimental procedures were approved by the Animal Policy and Welfare Committee of Wenzhou Medical University (Approval Number: wydw2021-0329).

4.7. Determination of proinflammatory cytokines IL-6 and TNF-α

The levels of IL-6 and TNF-α in the culture medium, serum, and BALF were detected using the ELISA kit according to the instructions of the manufacturer. In cell-based experiments, the data were normalized to the amount of total protein in lysates from the same culture.

4.8. Cytotoxicity assessment

J774A.1 macrophages were treated with the synthesized derivatives at a concentration of 10 μM for 24 h. Subsequently, MTT (5 mg/mL) was added to each well and incubated for 4 h. The absorbance at 490 nm was measured with a Bio-Rad multi-well plate reader.

4.9. Real-time quantitative reverse transcription PCR assay

The total RNA was isolated from cells or lung tissues with TRIzol. Total RNA concentration and purity were measured using the ultraviolet–visible spectrophotometer Nanodrop 2000 (Thermo Scientific, USA). RT-qPCR was performed using the M-MLV Platinum RT-qPCR kit with the Eppendorf Realplex4 instrument (Eppendorf, Hamburg, Germany). The transcript levels were normalized to those of the β-actin reference gene.

4.10. Western blotting

The J774A.1 macrophages were preincubated with **13a** (10, 5 μM) or vehicle control (DMSO) for 2 h and then incubated with LPS (0.5 μg/mL) for 30 min to activate NF-κB. The cells were then lysed with RIPA, and total protein was collected. The protein concentrations were determined using the Bradford assay. The protein samples were boiled in loading buffer at 100 °C for 10 min, separated with 12.5% SDS-PAGE, and transferred to the PVDF membrane. The PVDF membranes were blocked with 5% milk for 1.5 h and subsequently incubated with primary antibodies and secondary HRP-conjugated antibodies. Finally, the blots were detected using an ECL detection reagent.

4.11. Detection of NF-κB p65 translocation in cells

To assess NF-κB activation, staining for p65 translocation in the cells was performed using the cellular NF-κB P65 translocation tit according to the manufacturer's protocol.

4.12. Model of ALI

The mice were divided into four groups (n = 8 per group), which were designated as "control" (received 0.9% NaCl), "LPS" (received 5 mg/kg LPS), "LPS + **13a**" (received 20 mg/kg **13a** and 5 mg/kg LPS), and "LPS + DXMS" (received 20 mg/kg DXMS and 5 mg/kg LPS). The mice were orally perfused with **13a** and DXMS 30 min prior to the intratracheal perfusion of LPS. After 6 h of LPS challenge, the mice were sacrificed under chloral hydrate anesthesia. Lung tissue, serum, and BALF were collected and stored at −80 °C.

4.13. Lung histopathology

The upper lobe of the right lung was fixed with 4% paraformaldehyde and embedded in paraffin. The deparaffinized sections were stained with the H&E kits, and standard light microscopy protocols were used to assess the extent of lung injury.

The deparaffinized sections were stained with the macrophage markers F4/80. Briefly, 10 mM sodium citrate buffer (pH 6.5) was used to extract the antigen epitopes from the sections. After blocking the endogenous peroxidase with 3% H_2O_2, the deparaffinized sections were incubated with 5% BSA for 1 h and then with primary anti-F4/80 antibody for 12 h at 4 °C. The sections were later incubated with

HRP-conjugated secondary antibody for 15 min, colored with 3,3-diaminobenzidine hydrochloride, stained with hematoxylin, and observed microscopically.

4.14. Mouse model of sepsis

. The mice were divided into three groups (n = 12 per group), which were designated as "control" (received the same volume of 0.9% NaCl), "LPS" (received 20 mg/kg LPS), and "LPS + **13a**" (received 20 mg/kg **13a** and 20 mg/kg LPS). The mice were orally perfused with **13a** and DXMS 1 h before the intraperitoneal injection of LPS. Mouse survival and weight were observed every 12 h for 6 days.

4.15. Statistical analysis

The data from different groups were analyzed using GraphPad Prism 8.0 software (GraphPad, San Diego, CA). The relevant data were expressed as mean ± SEM. $P < 0.05$ was considered statistically significant.

Declaration of competing interest

The authors declare that they have no known competing financial interests or personal relationships that could have appeared to influence the work reported in this paper.

Data availability

No data was used for the research described in the article.

Acknowledgments

This study was funded in part with the funds provided by the National Natural Science Funding of China (21961142009, 82073705, 82273791), Thailand Research Fund Grant (DBG6280006), Zhejiang Provincial Key Scientific Project (2021C03041), Natural Science Funding of Zhejiang Province (LR22H300002), Qianjiang Talent Plan of Zhejiang (QJD1902016), Scientific Research Starting Foundation in Wenzhou Medical University (QTJ21013), and Research Fund from the University of Chinese Academy of Sciences (WIUCASQD2020016).

Appendix A. Supplementary data

Supplementary data to this article can be found online at https://doi.org/10.1016/j.ejmech.2023.115144.

References

[1] C.P. Dang, A. Leelahavanichkul, Over-expression of miR-223 induces M2 macrophage through glycolysis alteration and attenuates LPS-induced sepsis mouse model, the cell-based therapy in sepsis, PLoS One 15 (2020), e0236038.
[2] G. Bellani, J.G. Laffey, T. Pham, E. Fan, L. Brochard, A. Esteban, L. Gattinoni, F. van Haren, A. Larsson, D.F. McAuley, M. Ranieri, G. Rubenfeld, B.T. Thompson, H. Wrigge, A.S. Slutsky, A. Pesenti, L.S. Investigators, E.T. Group, Epidemiology, patterns of care, and mortality for patients with acute respiratory distress syndrome in intensive care units in 50 countries, JAMA 315 (2016) 788–800.
[3] N.T. Mowery, W.T.H. Terzian, A.C. Nelson, Acute lung injury, Curr. Probl. Surg. 57 (2020), 100777.
[4] D.C. Krutsinger, K.N. Yadav, M.O. Harhay, K. Bartels, K.R. Courtright, A systematic review and meta-analysis of enrollment into ARDS and sepsis trials published between 2009 and 2019 in major journals, Crit. Care 25 (2021) 392.
[5] M. Singer, C.S. Deutschman, C.W. Seymour, M. Shankar-Hari, D. Annane, M. Bauer, R. Bellomo, G.R. Bernard, J.D. Chiche, C.M. Coopersmith, R.S. Hotchkiss, M. M. Levy, J.C. Marshall, G.S. Martin, S.M. Opal, G.D. Rubenfeld, T. van der Poll, J. L. Vincent, D.C. Angus, The third international consensus definitions for sepsis and septic shock (Sepsis-3), JAMA 315 (2016) 801–810.
[6] K. Xiao, W. He, W. Guan, F. Hou, P. Yan, J. Xu, T. Zhou, Y. Liu, L. Xie, Mesenchymal stem cells reverse EMT process through blocking the activation of NF-kappaB and Hedgehog pathways in LPS-induced acute lung injury, Cell Death Dis. 11 (2020) 863.
[7] T. Ondee, J. Gillen, P. Visitchanakun, P. Somparn, J. Issara-Amphorn, C. Dang Phi, W. Chancharoenthana, D. Gurusamy, A. Nita-Lazar, A. Leelahavanichkul, Lipocalin-2 (Lcn-2) attenuates polymicrobial sepsis with LPS preconditioning (LPS tolerance) in FcGRIIb deficient lupus mice, Cells 8 (2019) 1064.
[8] H. Kumar, T. Kawai, S. Akira, Pathogen recognition by the innate immune system, Int. Rev. Immunol. 30 (2011) 16–34.
[9] H. Domscheit, M.A. Hegeman, N. Carvalho, P.M. Spieth, Molecular dynamics of lipopolysaccharide-induced lung injury in rodents, Front. Physiol. 11 (2020) 36.
[10] H. Yang, H. Lv, H. Li, X. Ci, L. Peng, Oridonin protects LPS-induced acute lung injury by modulating Nrf2-mediated oxidative stress and Nrf2-independent NLRP3 and NF-kappaB pathways, Cell Commun. Signal. 17 (2019) 62.
[11] S.T. Li, Q. Dai, S.X. Zhang, Y.J. Liu, Q.Q. Yu, F. Tan, S.H. Lu, Q. Wang, J.W. Chen, H.Q. Huang, P.Q. Liu, M. Li, Ulinastatin attenuates LPS-induced inflammation in mouse macrophage RAW264.7 cells by inhibiting the JNK/NF-kappaB signaling pathway and activating the PI3K/Akt/Nrf2 pathway, Acta Pharmacol. Sin. 39 (2018) 1294–1304.
[12] X. Chen, Y. Zhao, X. Wang, Y. Lin, W. Zhao, D. Wu, J. Pan, W. Luo, Y. Wang, G. Liang, FAK mediates LPS-induced inflammatory lung injury through interacting TAK1 and activating TAK1-NFkappaB pathway, Cell Death Dis. 13 (2022) 589.
[13] M. Zusso, V. Lunardi, D. Franceschini, A. Pagetta, R. Lo, S. Stifani, A.C. Frigo, P. Giusti, S. Moro, Ciprofloxacin and levofloxacin attenuate microglia inflammatory response via TLR4/NF-kB pathway, J. Neuroinflammation 16 (2019) 148.
[14] L-Citrulline for prevention of sequelae of acute lung injury in pediatrics undergoing cardiopulmonary bypass for heart defects. https://beta.clinicaltrials.gov/study/NCT02891837.
[15] The effect of Aspirin on REducing iNflammation in human in vivo model of acute lung injury (ARENA). https://beta.clinicaltrials.gov/study/NCT01659307.
[16] Ibuprofen in sepsis study. https://beta.clinicaltrials.gov/study/NCT00000574.
[17] Efficacy & safety of Resatorvid in adults with severe sepsis. https://beta.clinicaltrials.gov/study/NCT00143611.
[18] Y.Q. He, C.C. Zhou, L.Y. Yu, L. Wang, J.L. Deng, Y.L. Tao, F. Zhang, W.S. Chen, Natural product derived phytochemicals in managing acute lung injury by multiple mechanisms, Pharmacol. Res. 163 (2021), 105224.
[19] Y.L. Zhang, W.X. Zhang, J.Q. Yan, Y.L. Tang, W.J. Jia, Z.W. Xu, M.J. Xu, N. Chattipakorn, Y. Wang, J.P. Feng, Z.G. Liu, G. Liang, Chalcone derivatives ameliorate lipopolysaccharide-induced acute lung injury and inflammation by targeting MD2, Acta Pharmacol. Sin. 43 (2022) 76–85.
[20] X.M. Wang, J. Yang, B. Ding, P. Chen, Z.W. Xu, Y. Zhao, P. Chen, N. Chattipakorn, G. Liang, D. Wu, Q.D. Tang, Design, synthesis and bioactivity evaluation of fisetin derivatives as potential anti-inflammatory agents against LPS-induced acute lung injury, Bioorg. Med. Chem. 49 (2021), 116456.
[21] R. Tian, H. Zhu, Y. Lu, X. Shi, P. Tu, H. Li, H. Huang, D. Chen, Therapeutic potential of 2-methylquinazolin-4(3H)-one as an antiviral agent against influenza A virus-induced acute lung injury in mice, Molecules 27 (2022) 7857.
[22] Y. Li, X. Chen, H. Zhang, J. Xiao, C. Yang, W. Chen, Z. Wei, X. Chen, J. Liu, 4-Octyl itaconate alleviates lipopolysaccharide-induced acute lung injury in mice by inhibiting oxidative stress and inflammation, Drug Des. Dev. Ther. 14 (2020) 5547–5558.
[23] S. Hayashi, N. Ueno, A. Murase, Y. Nakagawa, J. Takada, Novel acid-type cyclooxygenase-2 inhibitors: design, synthesis, and structure-activity relationship for anti-inflammatory drug, Eur. J. Med. Chem. 50 (2012) 179–195.
[24] Y.Q. He, C.C. Zhou, L.Y. Yu, L. Wang, J.L. Deng, Y.L. Tao, F. Zhang, W.S. Chen, Natural product derived phytochemicals in managing acute lung injury by multiple mechanisms, Pharmacol. Res. 163 (2021), 105224.
[25] Z. Liu, L. Chen, P. Yu, Y. Zhang, B. Fang, C. Wu, W. Luo, X. Chen, C. Li, G. Liang, Discovery of 3-(Indol-5-yl)-indazole derivatives as novel myeloid differentiation protein 2/Toll-like receptor 4 antagonists for treatment of acute lung injury, J. Med. Chem. 62 (2019) 5453–5469.
[26] Z. Liu, L. Tang, H. Zhu, T. Xu, C. Qiu, S. Zheng, Y. Gu, J. Feng, Y. Zhang, G. Liang, Design, synthesis, and structure-activity relationship study of novel indole-2-carboxamide derivatives as anti-inflammatory agents for the treatment of sepsis, J. Med. Chem. 59 (2016) 4637–4650.
[27] C. Abdel Shaheed, G.E. Ferreira, A. Dmitritchenko, A.J. McLachlan, R.O. Day, B. Saragiotto, C. Lin, V. Langendyk, F. Stanaway, J. Latimer, S. Kamper, H. McLachlan, H. Ahedi, C.G. Maher, The efficacy and safety of paracetamol for pain relief: an overview of systematic reviews, Med. J. Aust. 214 (2021) 324–331.
[28] S.L.P. Scroggs, C.C. Andrade, R. Chinnasamy, S.R. Azar, E.E. Schirtzinger, E. I. Garcia, J.B. Arterburn, K.A. Hanley, S.L. Rossi, Old drugs with new tricks: efficacy of fluoroquinolones to suppress replication of flaviviruses, Viruses 12 (2020).
[29] M. Zusso, V. Lunardi, D. Franceschini, A. Pagetta, R. Lo, S. Stifani, A.C. Frigo, P. Giusti, S. Moro, Ciprofloxacin and levofloxacin attenuate microglia inflammatory response via TLR4/NF-κB pathway, J. Neuroinflammation 16 (2019) 148.
[30] K. Tabara, R. Tamura, A. Nakamura, S. Mori, T. Kitano, K. Fujikawa, M. Fujikawa, K. Okamoto, S. Kanayama, H. Uratsuji, F. Ikeda, T. Matsumoto, Anti-inflammatory effects of ozenoxacin, a topical quinolone antimicrobial agent, J. Antibiot. 73 (2020) 247–254.
[31] A. Duran, N. Valero, J. Mosquera, E. Fuenmayor, M. Alvarez, Gefitinib and pyrrolidine dithiocarbamate decrease viral replication and cytokine production in dengue virus infected human monocyte cultures, Life Sci. 191 (2017) 180–185.
[32] K. Ray, B. Ujvari, V. Ramana, J. Donald, Cross-talk between EGFR and IL-6 drives oncogenic signaling and offers therapeutic opportunities in cancer, Cytokine Growth Factor Rev. 41 (2018) 18–27.

[33] A.M. Alafeefy, A.A. Kadi, O.A. Al-Deeb, K.E. El-Tahir, N.A. Al-Jaber, Synthesis, analgesic and anti-inflammatory evaluation of some novel quinazoline derivatives, Eur. J. Med. Chem. 45 (2010) 4947–4952.
[34] Y. Zhang, J. Wu, S. Ying, G. Chen, B. Wu, T. Xu, Z. Liu, X. Liu, L. Huang, X. Shan, Y. Dai, G. Liang, Discovery of new MD2 inhibitor from chalcone derivatives with anti-inflammatory effects in LPS-induced acute lung injury, Sci. Rep. 6 (2016), 25130.
[35] Y. Zhang, T. Xu, Z. Pan, X. Ge, C. Sun, C. Lu, H. Chen, Z. Xiao, B. Zhang, Y. Dai, G. Liang, Shikonin inhibits myeloid differentiation protein 2 to prevent LPS-induced acute lung injury, Br. J. Pharmacol. 175 (2018) 840–854.
[36] L. Chen, H. Chen, P. Chen, W. Zhang, C. Wu, C. Sun, W. Luo, L. Zheng, Z. Liu, G. Liang, Development of 2-amino-4-phenylthiazole analogues to disrupt myeloid differentiation factor 88 and prevent inflammatory responses in acute lung injury, Eur. J. Med. Chem. 161 (2019) 22–38.
[37] S. Hirano, Q. Zhou, A. Furuyama, S. Kanno, Differential regulation of IL-1beta and IL-6 release in murine macrophages, Inflammation 40 (2017) 1933–1943.
[38] Y.W. Tsai, C.H. Lu, R.C. Chang, Y.P. Hsu, L.T. Ho, K.C. Shih, Palmitoleic acid ameliorates palmitic acid-induced proinflammation in J774A.1 macrophages via TLR4-dependent and TNF-alpha-independent signallings, Prostaglandins Leukot. Essent. Fatty Acids 169 (2021), 102270.
[39] L. Yang, W. Luo, Q. Zhang, S. Hong, Y. Wang, A.V. Samorodov, N. Chattipakorn, V. N. Pavlov, G. Liang, Cardamonin inhibits LPS-induced inflammatory responses and prevents acute lung injury by targeting myeloid differentiation factor 2, Phytomedicine 93 (2021), 153785.
[40] K. de Padua Lucio, A.C.S. Rabelo, C.M. Araujo, G.C. Brandao, G.H.B. de Souza, R. G. da Silva, D.M.S. de Souza, A. Talvani, F.S. Bezerra, A.J. Cruz Calsavara, D. C. Costa, Anti-inflammatory and antioxidant properties of black mulberry (morus nigra L.) in a model of LPS-induced sepsis, Oxid. Med. Cell. Longev. 2018 (2018), 5048031.
[41] Z. Ding, R. Zhong, Y. Yang, T. Xia, W. Wang, Y. Wang, N. Xing, Y. Luo, S. Li, L. Shang, Z. Shu, Systems pharmacology reveals the mechanism of activity of Ge-Gen-Qin-Lian decoction against LPS-induced acute lung injury: a novel strategy for exploring active components and effective mechanism of TCM formulae, Pharmacol. Res. 156 (2020), 104759.
[42] P. Chen, Z. Xu, X. Wang, J. He, J. Yang, J. Wang, N. Chattipakorn, D. Wu, Q. Tang, G. Liang, T. Chen, Discovery of new cinnamic derivatives as anti-inflammatory agents for treating acute lung injury in mice, Arch. Pharmazie (2022), e2200191.
[43] J. Ren, D. Su, L. Li, H. Cai, M. Zhang, J. Zhai, M. Li, X. Wu, K. Hu, Anti-inflammatory effects of Aureusidin in LPS-stimulated RAW264.7 macrophages via suppressing NF-kappaB and activating ROS- and MAPKs-dependent Nrf2/HO-1 signaling pathways, Toxicol. Appl. Pharmacol. 387 (2020), 114846.
[44] J. Tang, L. Xu, Y. Zeng, F. Gong, Effect of gut microbiota on LPS-induced acute lung injury by regulating the TLR4/NF-kB signaling pathway, Int. Immunopharm. 91 (2021), 107272.
[45] F.R. D'Alessio, Mouse models of acute lung injury and ARDS, Methods Mol. Biol. 1809 (2018) 341–350.
[46] F. Abedi, A.W. Hayes, R. Reiter, G. Karimi, Acute lung injury: the therapeutic role of Rho kinase inhibitors, Pharmacol. Res. 155 (2020), 104736.
[47] Y. Butt, A. Kurdowska, T.C. Allen, Acute lung injury: a clinical and molecular review, Arch. Pathol. Lab Med. 140 (2016) 345–350.
[48] S. Mukhopadhyay, J.R. Hoidal, T.K. Mukherjee, Role of TNFalpha in pulmonary pathophysiology, Respir. Res. 7 (2006) 125.
[49] R. Xiong, W. Jiang, N. Li, B. Liu, R. He, B. Wang, Q. Geng, PM2.5-induced lung injury is attenuated in macrophage-specific NLRP3 deficient mice, Ecotoxicol. Environ. Saf. 221 (2021), 112433.
[50] X. Li, C. Shan, Z. Wu, H. Yu, A. Yang, B. Tan, Emodin alleviated pulmonary inflammation in rats with LPS-induced acute lung injury through inhibiting the mTOR/HIF-1alpha/VEGF signaling pathway, Inflamm. Res. 69 (2020) 365–373.
[51] H. Chen, N. Huang, J. Li, J. Sun, L. Shi, C. Zhang, Y. Zhao, G. Kong, Z. Li, Immune suppression reversal of the spleen: a promising strategy for improving the survival rate of sepsis in rats, Am. J. Transl. Res. 13 (2021) 9005–9014.
[52] A. Zhang, E. Charles, J. Xing, R. Sawyer, Z. Yang, Pulsed ultrasound of the spleen prolongs survival of rats with severe with severe intra-abdomainal sepsis, J. Surg. Res. 259 (2021) 97–105.